https://doi.org/10.1016/j.jcsr.2021.106536

High Strength Steel Square and Rectangular Tubular Stub Columns Infilled with Concrete

Yancheng Cai [a], Meini Su [b,*], Xuerui Chen [b], Ben Young [a]

[a] Department of Civil and Environmental Engineering, The Hong Kong Polytechnic University, Hong Kong, China
(Formerly, Department of Civil Engineering, The University of Hong Kong, Pokfulam Road, Hong Kong, China)

[b] Department of Mechanical, Aerospace, and Civil Engineering, The University of Manchester, Manchester, UK

Abstract: This paper presents the experimental and numerical investigations of high strength steel square and rectangular tubular stub columns infilled with concrete. Firstly, a series of tests was conducted on cold-formed high strength steel (CFHSS) square and rectangular tubular sections infilled with three different concrete compressive strengths, i.e., 40, 80 and 120 MPa. The CFHSS tubular sections had the nominal 0.2% proof stress (yield stress) up to 900 MPa. Secondly, an extensive numerical study accounting for the confinement effect, as well as the non-linearities of materials, geometry and contacts was performed. Upon validation against the test results, a parametric investigation was conducted. The structural behaviour of concrete-filled CFHSS stub columns was investigated, including the ultimate load, end shortening, strength enhancement index and ductility index. Finally, the experimental and numerical results were used to assess the suitability of the design rules specified in the current American Specification (AISC) and European Code (EC4) for the compressive strength of the concrete-filled CFHSS square and rectangular stub columns. It was found that the predictions from EC4 were generally unconservative while those from the AISC were conservative. However, the predictions by EC4 became conservative if the effective strength of infilled concrete or the effective area of outer steel tubes were considered in the design. In addition, the predictions by EC4 became less scattered for different infilled concrete strengths when the effective concrete strengths were used. However, using the effective concrete strengths or the effective areas did not lead to the improvements of for the AISC specifications.

Keywords: Concrete-filled steel tube; experimental investigation; high strength steel; numerical investigation; square and rectangular hollow sections.

* Corresponding author.
E-mail address: Meini.su@manchester.ac.uk

1. Introduction

Concrete-filled steel tubular (CFST) members have been used widely in the construction industry for their excellent structural performance. They have been used as mega columns in super high-rise buildings [1], chord members in composite arch bridges [2], piles in floodwall structures [3], bridge piers [4] as well as submarine pipeline structures [5-6]. Their excellent structural performance is mainly benefited from the synergistic interactions between the inner concrete and the outer steel tube; for example, the steel tube provides confinement to the infilled concrete while the infilled concrete prevents the inward buckling and delays the local buckling of the steel tube [7]. These contribute to the structural behaviour of the concrete-filled members, e.g., increased bearing capacity and ductility for concrete-filled steel columns under axial loading condition. Hence, CFST steel columns may provide more economic efficiency than pure structural steel or reinforced concrete columns due to the reduced column size and increased effective space in buildings [8-9].

In the last few decades, experimental, numerical and analytical investigations have been carried out on the structural behaviour and practical applications of CFST columns under various loading conditions, as summarized in the recent literature [9-16]. There are two common methods to improve the load resistance of CFST columns [17] - by increasing the cross-section areas or using high strength materials. The first method might be impractical or uneconomic because the increased area will induce larger structural weight with less usable area and subsequently increase the cost of foundation. The second method of using high strength materials such as high strength steel and concrete could be a more effective way. In addition, the use of high strength steel allows for larger strain ranges of elastic behaviour and thus improving the confinement to the infilled concrete core [9].

With the advancements in material and fabrication techniques, high strength steels and concrete become available nowadays, for examples, in terms of the yield stress (f_y) of steel tubes greater than 1100 MPa [18] and the compressive strength of concrete (f_{ck}) up to 190 MPa [19]. These developments in individual constituent components have driven the investigations on the behaviour and design of higher performance composite structures, such as high strength steel tubes infilled with high strength concrete [17, 19-21]. A recent review by Liew *et al*. [9] on the CFST columns with over 2030 test results showed that more than 70% of the test data using normal strength concrete with f_{ck} not greater than 50 MPa, and over 90% of the data using mild steel with f_y not greater than 460 MPa. It should be noted that, up to date, investigations on the high strength steel tubes infilled with high strength concrete are relatively limited.

Design of CFST columns are available in current international design specifications, such as the "Eurocode 4: Design of Composite Steel and Concrete Structures - Part 1.1: General Rules and Rules for Buildings" (EC4) [22], the American Specification for Structural Steel Buildings (AISC) [23], the Japanese specification of "Recommendations for design and construction of concrete filled steel tubular structures" (AIJ) [24] and Australian/New Zealand Standard of "Composite structures - Composite steel-concrete construction in buildings" (AS/NZS2327) [25]. It should be noted that limitations of the design rules are specified in these specifications, in particular on the yield stress of steel and the compressive strength of concrete. However, the design of high strength square and

rectangular steel tubes infilled with high strength concrete are not explicitly specified in these design codes [22-25], for example, for columns with $f_y \geq 900$ MPa and $f_{ck} \geq 80$ MPa. This will be discussed further in the later section of this paper.

In this study, experimental and numerical investigations were carried out on the structural behaviour of concrete-filled cold-formed high strength steel (CFHSS) square and rectangular stub columns. Firstly, a comprehensive test program consisting of 34 specimens was carried out. The specimens were designed with CFHSS square and rectangular tubes infilled with three different compressive cylinder strengths (40, 80 and 120 MPa) of concrete. The CFHSS tubular sections had the nominal 0.2% proof stress ($f_{0.2}$) up to 900 MPa. The test specimens were subjected to uniform axial compression. The ultimate loads and failure modes were obtained. Secondly, an extensive numerical study accounting for the confinement effect, as well as the non-linearities of materials, geometry and contacts was performed. After a successful model validation against test results, a parametric study was conducted by using the validated numerical model. The specimens in the parametric study were designed to cover a wide range of the cross-section dimensions and section slenderness of the CFHSS tubes that infilled with different strengths of concrete. The structural behaviour of concrete-filled CFHSS stub columns was investigated, including the ultimate load, end shortening, strength enhancement index and ductility index. Finally, the experimental and numerical results were used to assess the suitability of the design rules specified in the current international specifications (EC4 [22] and AISC360-10 [23]).

2. Test program

2.1 Material properties

The CFHSS square and rectangular tubes were used as the outer skin of the concrete-filled steel stub column specimens. The nominal dimensions ($H \times B \times t$) of the steel tubes were 80×80×4.0 mm, 100×50×4.0 mm, 100×100×4.0 mm, 120×120×4.0 mm, 140×140×5.0 mm and 160×160×4.0 mm, where H, B and t are the outer depth, width and thickness of the tubes, respectively, as illustrated in Figure 1. The steel tubes of 80×80×4.0 mm and 100×100×4.0 mm had the nominal 0.2% proof stress ($f_{0.2}$) of 700 and 900 MPa, the steel tubes of 100×50×4.0 mm, 140×140×5.0 mm and 160×160×4.0 mm had the $f_{0.2}$ of 700 MPa and the steel tubes of 120×120×4.0 mm had the $f_{0.2}$ of 900 MPa. The CFHSS tubes were divided into two groups based on the nominal value of $f_{0.2}$, as shown in Table 1, where in the tube labelling, the letter "A" followed the hyphen of the section legend represents $f_{0.2}$ = 700 MPa, and the letter "B" stands for $f_{0.2}$ = 900 MPa.

The coupons were machined from the tubes at 90° angle from the weld. The nominal gauge length and width of the tensile coupons were 25 mm and 6 mm, respectively [18]. The coupon specimens were tested in a 50-kN MTS testing machine. Two linear strain gauges were adhered on both faces at the middle of the coupon. An extensometer was mounted on the coupons over a gauge length of 25 mm. Displacement control test method was used with loading rates of 0.05 mm/min and 0.5 mm/min for the elastic range and plastic range, respectively. The results from the strain gauges were used to

118 determine the Young's modulus (E_s) of the coupon specimens. The stress-strain curves of the CFHSS
119 tubular members are shown in Figures 2(a)-(b) for the members with nominal $f_{0.2}$ of 700 MPa and
120 900 MPa, respectively. The rest of the material properties were determined from the stress-strain
121 curves that measured by the extensometer. The results from coupon tests are presented in Table 1,
122 including the E_s, $f_{0.2}$, the ultimate strength (f_u), the strain at ultimate (ε_u), and the strain at fracture (ε_f).

123 Three different mixes of concrete (C40, C80 and C120) with the respective nominal compressive
124 cylinder strengths (f_{ck}) of 40 MPa, 80 MPa and 120 MPa were prepared to infill the steel tubes.
125 Concrete cylinders were prepared to determine the concrete strengths. The concrete cylinder had the
126 nominal diameter of 150 mm and height of 300 mm. The cylinder tests were conducted in accordance
127 with the procedures in the ACI [26]. Two series of cylinder compression tests were conducted to
128 obtain the cylinder strength (f_{ck}), one on the 28th day after casting and the other on the date of the
129 corresponding stub column tests [27]. The average test results of the different concrete mixes are
130 presented in Table 2.

131

132 *2.2 Test specimens*

133 A series of concrete-filled CFHSS square and rectangular stub column specimens were designed by
134 using the aforementioned seven types of CFHSS tubes (Table 1) as the outer skin. Each series of tubes
135 were infilled with those three different mixes of concrete (Table 2), namely, C40, C80 and C120. In
136 addition, to reflect the effects of infilled concrete in the same specimen series, the CFHSS square and
137 rectangular stub columns without infilled concrete were also designed. Hence, there are 34 stub
138 column specimens in this study, including two repeated specimens, as shown in Tables 3-4 for the
139 steel grades of outer tubes in Series A and B, respectively. The parameters of the specimens mainly
140 included the variations of $H/B = 1.0$ and 2.0, h/t ranging from 15.1 to 35.3 (h represents the flat portion
141 of the section height), the two steel grades (Series A and B) and the three different strengths of
142 concrete infill. The nominal length (L) of each CFHSS tube was taken as $3D$ in order to make sure
143 that each specimen would not fail by overall buckling. The mean values of the measured section
144 dimensions and lengths of the tubular stub column specimens were summarized in Tables 3-4. All the
145 steel square and rectangular tubes were wire cut at both ends before infilling concrete. Concrete of
146 different strengths was then cast into the steel tubes and vibrator was also used in the casting process.

147 The stub column specimens were labelled by distinguishing their nominal section dimensions,
148 nominal concrete cylinder strengths and the steel grades of outer tubes. For example, Specimen
149 100×100×4-C40-A, the first segment of 100×100×4 (H×B×t) indicates that the nominal section
150 dimensions of the outer tube, and the symbol following the hyphen indicates the steel tube is infilled
151 with concrete having the nominal cylinder compressive strength of 40 MPa. It should be noted that
152 the symbol "C0" means there is no infilled concrete, namely, it is a CFHSS stub column specimen
153 with hollow section. The last segment represents the nominal strengths of the steel tubes, where "A"
154 and "B" for the $f_{0.2}$ of 700 MPa and 900 MPa, respectively, as mentioned earlier. If it is a repeated
155 test, it is indicated by a letter "r" in the end of the label. The details of the concrete-filled CFHSS
156 square and rectangular tubular stub column specimens are shown in Tables 3-4.

2.3 *Test setup*

Tests of the concrete-filled CFHSS tubular stub columns were conducted in the Structural Laboratory at The University of Hong Kong. Figure 3 illustrates a typical test setup. A 5000 kN capacity servo-controlled hydraulic testing machine was used to apply axial compressive force to the concrete-filled CFHSS stub column specimens. Three 50-mm range Linear Voltage Differential Transducers (LVDTs) were used to measure the end shortening of the specimens. These three LVDTs were placed between the top and bottom bearing plates at evenly located positions. To prevent "elephant foot" failure, end-stiffeners (steel frames) with height of around 25 mm were used near each end of the column prior to testing. It should be noted that, for the stub columns infilled with concrete, the top surface of the column might not be at the same level as the end of the steel tube due to shrinkage of the concrete. Hence, plaster materials were used to fill the small gap between the steel tube and infilled concrete [27], as illustrated in Figure 4.

A special ball bearing was used at the top end of the specimen. An initial load of around 2 kN was applied to the specimens. During pre-loading, any possible gaps between the specimen and the contacting surfaces of the testing machine were eliminated. The bearing was then locked after pre-loading. Hence, the load was applied uniformly across the whole composite cross-section. Compressive load was applied by displacement control to the specimens with a constant rate of 0.2 mm/min using the servo-controlled hydraulic testing machine. By using this test method, the tests could be continued after experiencing the peak loads. The stub column tests were stopped when clear drops of axial loads were observed. A data logger was used to record the readings from the LVDTs and loads at the interval of 1 second. The load-end shortening responses of the test specimens were thus obtained.

2.4 *Test results*

The compressive behaviour of the stub columns was observed during the tests. The ultimate load (P_t) of the specimen and the corresponding end-shortening (δ_u), as well as the end-shortening ($\delta_{u,0.85}$) at $0.85P_t$ after each specimen experienced its ultimate load are shown in Tables 5-6, for CFHSS series A and B, respectively. The applied load versus axial end-shortening relationship was obtained for each column specimen (e.g., curves in Figures 5(a)-(d)), where the applied load was recorded from the actuator and the end-shortening was taken as the average readings of three LVDTs. Two repeated tests were conducted (i.e. 100×50×4-C40-A-r and 120×120×4-C80-B-r), and the ultimate loads of the repeated tests were very close to their respective first test results, with a maximum difference of 1.9%. This small difference indicated the reliability of the test results. The ultimate loads (P_t) of the concrete-filled stub column specimens were normalized with those ($P_{t,0}$) without infilled concrete for the same series, indicated by the abbreviation of "*Nor.*", as shown in Tables 5-6. It is clearly shown that the ultimate loads of the tubular specimens were significantly improved by the infilled concrete in this study, for examples, up to 326% for Series 160×160×4-A and up to 211% for Series 120×120×4-B.

All the concrete-filled CFHSS square and rectangular stub columns failed by the crushing of the infilled concrete together with outward buckling of the steel tubes at some locations. It should be noted that the use of steel frames at the ends of the columns was able to prevent the "elephant foot" failure of the specimens. The local buckling failure was observed for all specimens. The inward and outward local buckling behaviour was found in specimens without infilled concrete, i.e., specimens of 80×80×4-C0-A, 100×50×4-C0-A (see Figure 6), 100×100×4-C0-A, 140×140×5-C0-A, 160×160×4-C0-A, 80×80×4-C0-B, 100×100×4-C0-B and 120×120×4-C0-B. However, the inward local buckling phenomenon was not observed in all concrete-filled CFHSS square and rectangular stub columns, as it was prevented by the infilled concrete in the steel tubes. Figures 6-7 further illustrate the failure modes of the tested concrete-filled CFHSS rectangular stub column Series 100×50×4-A and square stub column series 80×80×4-A and 80×80×4-B.

3. Finite element analysis

3.1 Development of model

Finite element model (FEM) was developed to simulate the tests of concrete-filled CFHSS square and rectangular stub column specimens. A finite element analysis software ABAQUS [29] was used to develop the FEM. The measured specimen dimensions (Tables 3-4), and material properties of the steel (Table 1) and concrete (Table 2) presented in Section 2 of this paper were used in the analysis of FEM.

The steel tube and concrete core were assigned by the S4R (four-node shell element with reduced integration) and the C3D8R (8-node linear brick element with reduced integration and hourglass control), respectively. Based on the mesh convergence study, the element mesh size of (B+D)/30 for the steel tube and (B+D)/15 for the concrete core was used. The engineering stress-strain (σ-ε) curve was converted to a true stress (σ_{true}) and logarithmic plastic strain (ε_{true}^{pl}) curve, by using the following Equations (1)-(2):

$$\sigma_{true} = \sigma(1 + \varepsilon) \quad (1)$$

$$\varepsilon_{true}^{pl} = ln(1 + \varepsilon) - \frac{\sigma_{true}}{E_s} \quad (2)$$

The true stress-true plastic strain curves were simplified by means of a piecewise linear stress-strain model, in particular, over the strain-hardening region.

The interactive behaviour between the steel tube and concrete was simulated using the interaction algorithm in ABAQUS [29]. The inner surface of the steel tube and the outer surface of the infilled concrete were defined to be a contact pair, of which the former acted as slave surface and the latter acted as master surface. Previous investigations [30] have shown that a friction coefficient from 0.1 to 0.5 generally causes limited effect on the prediction of the ultimate strength, but a smaller friction factor may induce a convergent problem with large deformation. It should be noted that different friction coefficients have been used in literature, for examples, coefficients of 0.25 [31], 0.3 [32] and

0.6 [33]. In the present study, the friction factor of 0.25 in the tangential direction between the concrete and steel was employed, while the "hard contact" behaviour in the normal direction was assumed with no penetration allowed between the surfaces.

Local imperfections were considered in the FEM of the square and rectangular tubular stub column specimens without infilled concrete (specimens of 80×80×4-C0-A, 100×50×4-C0-A, 100×100×4-C0-A, 140×140×5-C0-A, 160×160×4-C0-A, 80×80×4-C0-B, 100×100×4-C0-B and 120×120×4-C0-B), as those FEM for CFHSS square and rectangular tubular stub columns performed by Ma *et al*. [34]. However, local imperfections of steel tubes for concrete-filled CFHSS square and rectangular stub columns were not considered. This is because the influence of local imperfections on the behaviour of concrete-filled steel stub columns is negligible due to the infilled concrete. This has been proved by the sensitivity study for the effects of imperfections on the structural behaviour of concrete-filled stainless steel and carbon steel tubular stub columns, as detailed in Tao *et al*. [35-36]. Hence, unlike the FEM for CFHSS square and rectangular tubular stub columns [34], the initial imperfections of steel tubes were not considered in the FEM for the concrete-filled CFHSS stub columns in the present study.

A reference node located at the centroid of the cross-section for each column end was defined. The reference node was coupled with the corresponding cross-section at each column end in displacements and rotations. The reference nodes were restrained against all degrees of freedom, except for the longitudinal displacement (along the length direction of the stub column) at the loading point. A specified axial displacement was assigned to the reference node at the loading point. General Static analysis step was adopted [29]. Hence, the adopted displacement control method in the tests was simulated in the FEM analyses. The nonlinear geometric parameter (NLGEOM) was enabled to deal with the large displacement analysis.

3.2 Stress-strain of the confined concrete model

The lateral expansion of the infilled concrete is confined by the outer steel tube when the stub columns subjected to axial compression. This confinement helps to increase the strength and ductility of concrete, which refers as "composite action" between the steel tube and infilled concrete [37]. In this study, the confined model of concrete proposed by Tao *et al.* [38] was adopted in the FEM.

The key parameters in determining the "concrete damaged plasticity" of the confined concrete model were summarized in the following. The dilation angle (ψ) was assumed to be a constant value of 40° for concrete filled steel stub square and rectangular columns, as suggested by Tao et al. [38]. The flow potential eccentricity and viscosity parameters were taken as -1.0 and 0, respectively. The ratio of the compressive strength under biaxial loading to uniaxial compressive strength f_{b0}/f_{ck} was determined by $1.5f_{ck}^{-0.075}$, as suggested by Papanikolaou and Kappos [39]. Hence, in the validation of the FEM, the actual ratios of f_{b0}/f_{ck} for concrete of C40, C80 and C120 were taken as 1.148, 1.074 and 1.051, respectively, based on the respective measured compressive strengths of 35.5 MPa, 85.7 MPa and 114.9 MPa, as shown in Table 2. The ratio of the second stress invariant on the tensile

meridian to that on the compressive meridian (K) is one of the important parameters for determining the yield surface of concrete plasticity model. It is commonly taken from 0.5 to 1.0 by the researchers while the default value is 2/3 in ABAQUS [29]. In this study, the equation proposed by Yu *et al.* [40] was used to calculate the ratio of K. Thus, the values of K were 0.72, 0.71 and 0.70 for concrete compressive cylinder strengths of 40, 80 and 120 MPa, respectively. In addition, the fracture energy (G_F) was determined based on the reference [41-42], which are 0.068, 0.11 and 0.143 for concrete of C40, C80 and C120, respectively.

As mentioned previously, the stress-strain model (three stages) of the infilled concrete that considering the strain hardening/softening rule of concrete core proposed by Tao *et al.* [38] was used in this study, as illustrated in the following.

The initial stage ($0 < \varepsilon \leq \varepsilon_{c0}$) of the curve was determined by Equation (3):

$$\frac{\sigma}{f_{ck}} = \frac{A \cdot X + B \cdot X^2}{1 + (A-2)X + (B+1)X^2} \qquad 0 < \varepsilon \leq \varepsilon_{c0} \tag{3}$$

in which $X = \varepsilon/\varepsilon_{c0}$; $A = E_c\varepsilon_{c0}/f_{ck}$; $B = (A\text{-}1)^2/0.55 - 1$; E_c is the Young's modulus of the infilled concrete; ε_{c0} is the strain at peak stress under uniaxial compression determined by using Equation (4).

$$\varepsilon_{c0} = 0.00076 + \sqrt{(0.626 f_{ck} - 4.33) \times 10^{-7}} \tag{4}$$

In the second stage ($\varepsilon_{c0} < \varepsilon \leq \varepsilon_{cc}$) of the curve, the relationship of stress-strain was determined by the following Equations (5) and (6):

$$\frac{\varepsilon_{cc}}{\varepsilon_{c0}} = e^k \tag{5}$$

$$k = (2.9224 - 0.00367 f_{ck})\left(\frac{f_B}{f_{ck}}\right)^{0.3124 + 0.002 f_c} \tag{6}$$

where f_B represents the confining stress in concrete at strain of ε_{cc}. The confining stress of f_B was determined by Equation (7):

$$f_B = \frac{0.25(1 + 0.027 f_{0.2}) e^{\frac{-0.02\sqrt{B^2 + D^2}}{t}}}{1 + 1.6 e^{-10} (f_{ck})^{4.8}} \tag{7}$$

The last stage ($\varepsilon_{cc} < \varepsilon$), i.e., descending branch, of the stress-strain curve was determined by Equation (8):

$$\sigma = f_r + (f_{ck} - f_r) exp[-\left(\frac{\varepsilon - \varepsilon_{cc}}{\alpha}\right)^{\beta} \qquad \varepsilon \geq \varepsilon_{cc} \tag{8}$$

where f_r is the residual stress as determined by Equation (9). The parameters α and β are the factors that influence the shape of curve.

$$f_r = 0.1 f_{ck} \tag{9}$$

The parameter α is calculated as:

$$\alpha = 0.005 + 0.0075\xi_c \quad (10)$$

The parameter β is taken as 0.92 for concrete-filled square and rectangular steel stub columns [43].

3.3 Validation of FEM

Based on the developed FEM by using the measured dimensions and material properties, the modelling parameters as well as the confined concrete model, the analysis of the FE were performed. The developed FEM was validated by comparing the FE results with the test results in terms of the ultimate loads, failure modes and the load-end shortening curves. The comparison of the ultimate loads (P_t) from tests with those (P_{FEA}) predicted from the FE analysis are shown in Table 7. The mean value of the P_t/P_{FEA} is 1.00 with the corresponding coefficient of variation (COV) of 0.079. It is shown that the developed FEM can successfully replicate the ultimate capacities of the concrete-filled CFHSS square and rectangular stub columns. Figures 8-9 illustrate the comparison of load-end shortening curves and failure modes obtained from the test and FEA for specimens 80×80×4-C80-A and 120×120×4-C120-B, respectively. The contributions of the outer steel tubes and the concrete infill in the history of the load-end shortening curves that obtained from the FEA were also plotted in the figures. It is clearly shown that the infilled concrete reached its ultimate load (or first peak) earlier than that of the outer steel tube, as reflected in the smaller end shortening values. However, due to the confinement effect, the load resistance of the infilled concrete may increase as the end shortening increased even the load resistance of the outer steel tube reduced due to local buckling. Generally, it is shown that the end-shortenings (δ_u) of the concrete-filled CFHSS stub columns at the ultimate loads (or first peaks) were dominated by those of the concrete infill, namely, the values of end shortening for the concrete-filled CFHSS stub columns were close to those of the infilled concrete at the ultimate loads (or first peaks).

4. Parametric study

4.1 Design of specimens

The validated FEM was used to perform a further study on the behaviour of concrete-filled CFHSS square and rectangular stub columns. The parameters that may affect the structural behaviour of the stub columns were considered, including the cross-section dimensions, section slenderness (ratios of h/t), $f_{0.2}$ of the steel tubes (steel grades), compressive strengths of infilled concrete. A total of 52 specimens were carefully designed to cover a wide range of parameters, including 24 for rectangular specimens and 28 for square specimens. The ratios of h/t varied from 35.0 to 75.0 and from 10.0 to 55.0 for rectangular and square tubes, respectively. The stress-strain curves of sections 100×100×4-A and 100×100×4-B having the respective nominal $f_{0.2}$ of 700 MP and 900 MPa were used. As those of the test specimens, the compressive cylinder strengths (f_{ck}) of the infilled concrete were 40, 80 and 120 MPa, respectively, and the length of each stub column was taken to be 3D. The dimensions of concrete-filled CFHSS square and rectangular stub columns used in this parametric study are detailed

in Tables 8-9, respectively. The criterion for the specimen labelling is the same as those described in Section 2.2 of this paper. In this sense, the last letters "A" and "B" in the specimen labelling represent the different steel grades by using stress-strain curves of sections 100×100×4-A ($f_{0.2}$ = 700 MPa) and 100×100×4-B ($f_{0.2}$ = 900 MPa), respectively. The CFHSS stub columns without infilled concrete are also included, as distinguished by the segment of "C0".

4.2 Definition of parameters

The parametric study of the concrete-filled CFHSS square and rectangular stub columns aims to study its structural behaviour under axial compression. These included the ultimate load, end shortening, the strength enhancement index (***SI***), as well as the ductility index (***DI***) [28].

The strength enhancement index (***SI***), as expressed in Equation (11), is defined by the ratio of the ultimate compressive load (P_u) of the concrete-filled steel tubular stub column to the sum of the strengths of the individual constituent components (i.e., the concrete core and steel tube). The parameter ***SI*** reflects the contribution of composite action in concrete-filled CFHSS square and rectangular stub columns. A ***SI*** value higher than 1.0 indicates that the positive interaction between the steel hollow section and the concrete core was achieved. The positive interaction benefits from the confinement effect of the concrete core from the steel tube, as well as the contribution of the concrete core to the delay or elimination of the local buckling in the steel tubular hollow section.

$$\boldsymbol{SI} = P_u/(f_{0.2}A_s + f_{ck}A_c) \tag{11}$$

where A_s and A_c correspond to the cross-section areas of the outer steel tube and the concrete core. The ductility index (***DI***), as expressed in Equation (12), is defined as the ratio of $\delta_{u,0.85}$ to δ_u. The higher value of the parameter ***DI*** represents that the better ductility of the specimens.

$$\boldsymbol{DI} = \delta_{u,0.85}/\delta_u \tag{12}$$

4.3 Influence of parameters

The parametric study results are presented in Tables 8-9, including P_{FEA}, δ_u and $\delta_{u,0.85}$ for the concrete-filled CFHSS square and rectangular stub column specimens. The stub column specimens without infilled concrete (specimens H×B×t-C0-A and H×B×t-C0-B), which had the same nominal section sizes as those specimens with the infilled concrete, were also included. In addition, the ultimate loads of the concrete-filled CFHSS square and rectangular stub column specimens were normalized by the ultimate load ($P_{FEA,0}$) of the CFHSS tubular specimen (without infilled concrete) in the same series, as indicated by "*Nor.*" in the Tables 8-9, respectively. The normalized column strengths from the tests and FEA were plotted against the infilled concrete strengths associated with different steel grades (series A and B) and the ratios of h/t, as shown in Figures 10(a)-(c). Generally, it is shown that the normalized column strength increased linearly with the increment of the infilled concrete strength for the CFHSS square and rectangular stub column specimens with a given value of h/t (Figures 10(a)-

(c)), where the infilled concrete strength of "0" in the horizontal axis means the CFHSS square and rectangular hollow section columns without any infilled concrete. Similar findings have been presented by Su *et al.* [27] for concrete-filled CFHSS circular tubular stub columns and by Cai *et al.* [28] for concrete-filled cold-formed and hot-finished steel elliptical tubular stub columns.

The behaviour of the concrete-filled CFHSS square and rectangular stub column specimens was investigated in terms of the parameters of ***SI*** and ***DI*** based on the results from the tests and FEA, as shown in Tables 5-6 and Tables 8-9. Figure 11 presents the relationships between the strength enhancement index (***SI***) and ratios of h/t for stub columns with square sections. As shown in Figure 11, under a given infilled concrete strength, the value of ***SI*** decreased regularly as the value of h/t increased. The decrements for the infilled concrete with nominal f_{ck} of 40 MPa are more obvious than those infilled with nominal f_{ck} of 120 MPa. Similar trends were found for those stub column specimens with rectangular sections as illustrated in Figure 12. Furthermore, for the stub columns with square and rectangular sections, it was found that the value of ***SI*** generally decreased with the increment of the infilled concrete strength under the same value h/t when $h/t \leq 25.0$; however, when $h/t \geq 25.0$, the value of ***SI*** increased with the increment of the infilled concrete strength for a given value of h/t, as shown in Figures 11-12. Meanwhile, the values of ***SI*** that larger than 1.00 tended to be smaller than 1.00 as the ratio of h/t became larger, e.g., $h/t \geq 35$ for specimens with rectangular sections. One of the main reasons is due to the changing of the section slenderness, a larger value of h/t (i.e., from compact to slender) would fail in local buckling earlier and thus provide less confinement effect to the concrete core, which subsequently decreasing the section capacity.

The ductility indexes (***DI***) of the CFHSS square and rectangular stub columns with and without infilled concrete were also investigated, as presented in Tables 5-6 and Tables 8-9. As shown in the tables, the values of ***DI*** for the concrete-filled CFHSS square and rectangular e stub column specimens were generally higher than those of specimens without infilled concrete, except for those square and rectangular specimens with larger value of h/t, e.g., specimens with $h/t = 55.0$. This could be due to load resistance drops largely as the failure of local buckling in the outer steel tube occurs. However, these test and FE results indicated that the ductility of the CFHSS square and rectangular stub column specimens could be significantly enhanced by the infilled concrete, as discussed in the Section 1 of this paper.

5. Existing design rules

5.1 General

Design of concrete-filled steel square and rectangular stub columns are provided by the existing international design specifications [22-25], as mentioned in Section 1 of this paper. It should be noted that concrete grades over C60 are beyond the upper limit of the specified concrete grade in EC4 [22], where the strength classes of the normal weight concrete used in composite members range from C20/C25 to C50/C60 only. The design rules provided in EC4 [22] apply to steel grades from S235 (f_y = 235 MPa) to S460 (f_y = 460 MPa). The design rules specified in AISC [23] are applicable to CFST

members with $f_y \leq 525$ MPa and $21 \leq f_{ck} \leq 69$ MPa. The AIJ Specification [24] allows the steel yield stress and concrete compressive cylinder strength of 440 MPa and 90 MPa, respectively while the AS/NZS2327 [25] allows steel yield stress not greater than 690 MPa and concrete cylinder compressive strength in the range of 20 MPa to 100 MPa. In the present study, the existing design rules specified in EC4 [22] and AISC [23] were selected to calculate the nominal strengths of concrete-filled CFHSS square and rectangular stub columns. In addition, the recent proposal on the strength reduction of high strength concrete in concrete-filled steel tubular members [8] due to the effects of infilled concrete strength was also incorporated in the calculations, for the nominal strengths predicted by the aforementioned design specifications [22-23].

5.2 Eurocode 4: Design of Composite Steel and Concrete Structures (EC4)

EC4 [22] covers the design rules for encased, partially encased and concrete-filled columns both with and without reinforcements. In the present study, no reinforcement was used in the concrete-filled CFHHS stub columns. The compressive design resistance of concrete-filled square and rectangular sections in EC4 [22] is a simple summation of the steel tube and concrete contributions. Account is taken of the higher resistance of the concrete, which is caused by confinement from the outer steel tube, by adopting a concrete coefficient of 1.0, rather than 0.85, as specified in Section 6.7.3.2 in EC4 [22]. The cross-section capacity (P_{EC}) of a concrete-filled steel square and rectangular tubular stub column is thus given by Equation (13)

$$P_{EC} = A_s f_{0.2} + A_c f_{ck} \tag{13}$$

A slenderness limit of $H/t \leq 52(235/f_{0.2})^{\wedge 0.5}$ for the outer steel tube is specified in the Table 6.3 of EC4 [22]. It should be noted that the yield strength (f_y) of the steel tube was replaced by the 0.2% proof stress ($f_{0.2}$) of the CFHSS stubs in the present study. Beyond the slenderness limit, local buckling needs to be explicitly accounted for, but is not specified in EC4 [22]. Hence, a further investigation was recommended to determine a more appropriate limit for concrete-filled tubes [42]. In this study, for the cross sections exceeding the slenderness limit of $52(235/f_{0.2})^{\wedge 0.5}$, the effective width equations provided in EC3-1.5 [43], as given by the following Equations (14) and (15), were adopted to calculate the effective area of the outer steel tubes.

$$\rho \leq \frac{\bar{\lambda}_p - 0.055(3+\varphi)}{\bar{\lambda}_p^2} \leq 1.0 \quad \text{for } \bar{\lambda}_p > 0.5 + \sqrt{0.085 - 0.055\varphi} \tag{14}$$

$$\bar{\lambda}_p = \frac{(H-3t)/t}{28.4\varepsilon\sqrt{k_\sigma}} \tag{15}$$

where ρ = reduction factor for local buckling for plate buckling; φ is the stress ratio which equals to 1.0 in this study; $\bar{\lambda}_p$ is the plate slenderness; k_σ is the buckling factor corresponding to the φ and boundary conditions and k_σ = 4.0 in this study according to Table 4.1 in EC3-1.5 [43]; H is the flat height of the outer steel tube (replaced by B for the flat width). In the present study, for the test specimens and numerical specimens (shown in Tables 10-11) that exceed the above slenderness limit

of 52.0, the reduction factor ρ was used in the calculation of the cross-section area instead of the full cross-section area. Similar approach was also adopted by Wang *et al*. [42] to determine the cross-section strength of concrete-filled double skin rectangular stub columns.

Recently, investigations on the effects of concrete strength for concrete-filled steel short columns revealed that the complexity and severity increased as the infilled concrete strength increased [8]. In particular, it was found that for ultra-high strength concrete with f_{ck} > 90 MPa, the increment of concrete strength due to the confinement effect from steel tube should be ignored [9]. Based on the calibrations against the design rules in EC4 [22], a reduction factor (η) for the effective compressive strength of the infilled concrete in steel tubes was proposed, as shown in Equation (16). The formula has been used in the predictions of concrete-filled steel tubular stub columns where the effects of infilled concrete strength was considered, such as by Wei *et al.* [17] and Wang *et al.* [43]. The reduction factor was also employed in the calculation of concrete-filled steel square and rectangular stub columns in this study when the effects of infilled concrete strengths was considered.

$$\eta = \begin{cases} 1.0 - \frac{(f_{ck}-50)}{200} & 50\ \text{MPa} < f_{ck} \leq 90\text{MPa} \\ 0.8 & f_{ck} > 90\text{MPa} \end{cases} \quad (16)$$

5.3 Specification for Structural Steel Buildings (AISC)

The nominal compressive strength (P_{AISC}) of concrete-filled steel square and rectangular tubular sections under axial loading refers to the design rules specified in Section I2.2b in AISC [23]. For the cross-section strengths of concrete-filled steel square and rectangular stub columns, sections are categorized as compact, non-compact or slender according to the width-to-thickness ($\lambda = h/t$) ratios of the outer tubes, as specified in Section I1.4 and Table I1.1a of AISC [23]. The value of P_{AISC} was determined by Equations (17)-(19):

For compact sections ($\lambda \leq \lambda_p$),

$$P_{AISC} = P_p \quad (17a)$$

$$P_p = f_{0.2}A_s + 0.85f_{ck}A_c \quad (17b)$$

$$\lambda_p = 2.26\sqrt{E_s/f_{0.2}} \quad (17c)$$

where P_p is the compressive strength of compact sections; λ_p is the slenderness limit for determining whether a section is compact or non-compact.

For non-compact sections ($\lambda_p < \lambda \leq \lambda_r$),

$$P_{AISC} = P_p - \frac{P_p - P_y}{(\lambda_r - \lambda_p)^2}(\lambda - \lambda_p)^2 \quad (18a)$$

$$P_y = f_{0.2}A_s + 0.7f_{ck}A_c \quad (18b)$$

$$\lambda_r = 3.00\sqrt{E_s/f_{0.2}} \quad (18c)$$

where P_y is the compressive strength of non-compact sections; λ_r is the slenderness limit for determining whether a section is non-compact or slender.

For slender sections ($\lambda_r < \lambda \leq \lambda_{limit}$),

$$P_{no} = f_{cr}A_s + 0.7f_{ck}A_c \quad (19a)$$

$$f_{cr} = 9E_s(\frac{t}{b})^2 \quad (19b)$$

$$\lambda_{limit} = 5.00\sqrt{E_s/f_{0.2}} \quad (19c)$$

where f_{cr} is the compressive strength of slender sections. In the present study, all the CFHSS square and rectangular specimens are categorized as compact, non-compact or slender sections based on the above criterion except specimen Series 320×160×4-B in the parametric study, whose section slenderness (λ) exceeds the limit of $5.00(E_s/f_{0.2})^{0.5}$. Since the section slenderness beyond this value is not explicitly specified in the AISC [23], the reduction factor in Equation (14) for the effective cross-section area is also adopted in the calculation of the nominal strengths (P_{AISC}) for the specimen Series 320×160×4-B.

6. Assessment of codified strength predictions

6.1 General

The ultimate load (P_u) from the experimental (P_t) and numerical results (P_{FEA}) were compared with the nominal strengths predicted by the aforementioned design specifications [22-23], as summarized in Tables 10-11 and Figures 13-16. Comparisons were performed with all safety factors set to unity. In the comparisons, the specimens without infilled concrete were not included, as this study mainly focused on the structural behaviour of concrete-filled CFHSS column specimens with square and rectangular sections.

In the calculation of the nominal strengths (unfactored design strengths) for the test specimens, measured values of the material properties (Table 1) and specimen dimensions (Tables 3-4) were used, which enables a direct comparison between test results and compressive strengths predicted from existing design rules. In calculating the compressive strength of the test specimens, the concrete cylinder strength at the day of the stub column test were used (Table 2). The stress-strain curves of cold-worked materials did not possess sharp yield points. Hence, the measured 0.2% proof stress ($f_{0.2}$) was used as the yield strength (f_y) in calculating the compressive strength for the test specimens. For specimens generated in the parametric study, the measured $f_{0.2}$ of sections 100×100×4-A and 100×100×4-B were used for specimen using steel grades of series A ($f_{0.2}$ = 700 MPa) and B ($f_{0.2}$ = 900 MPa), respectively. The nominal cylinder strengths of the concrete were used. This is because, in the FE model for the parametric study, measured stress-strain curves of the CFHSS sections 100×100×4-A and 100×100×4-B were used together with the stress-strain curves obtained from the confined concrete model that were developed based on nominal concrete strengths.

6.2 *Predictions by EC4*

Table 10 shows the comparison of the test and FE strength-to-predicted strength by EC4 [22] for stub columns with square and rectangular section specimens. The relationships between the comparisons with EC4 [22] and the section slenderness values were plotted in Figures 13-14 for specimens with square and rectangular sections, respectively. Overall, predictions from EC4 [22] were generally unconservative as the mean values for the ratios of the P_u/P_{EC} were smaller than 1.00. As the CFHSS tubular sections became more slender, larger values of $H/t(f_{0.2}/235)^{0.5}$, the predictions generally became more unconservative. The modified predicted strength, P_{EC*}, represents that effective cross-section area of the steel tube was considered in the calculation of the cross-section area for those sections exceed the slenderness limit of $H/t(f_{0.2}/235)^{0.5}$ = 52.0. Under this circumstance, the predictions by EC4 [22] became conservative, with the mean values of P_u/P_{EC*} equalled to 1.07 and 1.09 for specimens with square and rectangular sections, respectively. Furthermore, the coefficients of variation (COV) were significantly reduced, for example in the predictions of specimens with rectangular sections, COV of 0.059 for P_u/P_{EC*} compared with that of 0.141 for P_u/P_{EC}. It means that the consideration of using effective section area for the specimens exceed the slenderness limit in EC4 [22] improved the strength predictions as the predictions became safer and less scattered. As mentioned in Section 5.2, the reduction factor of η, using Equation (16), for the effective compressive strength of the infilled concrete was also considered in the design predictions, as represented by $P_{EC\wedge}$ in Table 10. It is shown that the predictions were slightly improved as reflected in the mean values $P_u/P_{EC\wedge}$ closer to 1.00 with smaller values of COV. The predictions by EC4 [22] were further modified by considering both the reduction factor of ρ for the effective cross-section area of steel tube and the reduction factor of η for the effective compressive strength of the infilled concrete, as represented by $P_{EC*\wedge}$ in Table 10. The predictions by $P_{EC*\wedge}$ became more conservative than those by P_{EC}, P_{EC*} and $P_{EC\wedge}$, as reflected by the largest mean values; however, less scattered predictions were achieved as shown in the smaller values of corresponding COV, which was comparable with those of P_u/P_{EC*}. The specimens were divided into two groups based on the steel grades of series A and B for the outer steel tubes, it was found that EC4 [22] provided relatively more conservative predictions for those specimens with relatively lower steel grade for both square and rectangular specimens, namely, steel Series A with nominal $f_{0.2}$ = 700 MPa.

6.3 *Predictions by the AISC*

Table 11 shows the comparison of the test and FE strength-to-predicted strength by AISC [23] for stub columns with square and rectangular section specimens. The relationships between the comparisons with AISC [23] and the section slenderness values were plotted in Figures 15-16 for square and rectangular specimens, respectively. On the contrary, the predictions from AISC [23] were overall conservative, i.e., the mean values (P_u/P_{AISC}) of 1.18 and 1.09 for the square and rectangular specimens, respectively. It should be noted that the section slenderness of rectangular specimen Series 320×160×4-B exceeded the value of λ_{limit} [23], limit of $5.00(E_s/f_{0.2})^{0.5}$, hence, the reduction factor ρ in Equation (16) was incorporated in the calculation of the cross-section area (A_s) of the steel tube in the strength prediction, as distinguished by "#" for the values in the bracket in Table 11. Similarly,

the reduction factor of η for the effective compressive strength of the infilled concrete was also considered in the design predictions, as represented by modified predictions $P_{AISC\wedge}$ in Table 11. It is shown that generally, the modified predictions were not improved for AISC [23]. This may be due to the reduction factor (η) was proposed based on the design rules in EC4 [22]. The specimens were also divided into two groups based on the steel grades (i.e. series A and B) for the outer steel tubes. The AISC [23] provided relatively more conservative and more scattered predictions for those specimens with relatively higher steel grade (Series B with $f_{0.2}$ = 900 MPa) for rectangular specimens, however, relatively more conservative with less scattered predictions were provided for those specimens with relatively lower steel grade (Series A with $f_{0.2}$ = 700 MPa) for square specimens. Due to the limited numbers of specimens that exceeded the section slenderness limit (λ_{limit}), the specimens using the effective cross-section area instead of full cross-section area in the calculation were not plotted. As shown in Figures 15-16, for both square and rectangular sections, the predictions by AISC [23] were generally conservative for compact sections ($\lambda \leq \lambda_p$), however, for the non-compact ($\lambda_p < \lambda \leq \lambda_r$) and slender sections ($\lambda_r < \lambda \leq \lambda_{limit}$) as well as those beyond the slenderness limit ($\lambda_{limit} < \lambda$), the predictions became more conservative as the section slenderness increased.

6.4 Effects of infilled concrete strengths and section slenderness

Tables 12 (a)-(b) presents the summary of the comparisons between test and FE strengths with codified predictions [22-23] for square and rectangular sections, respectively. In each section type in each table, the specimens were divided by the different strengths of infilled concrete. For the predictions by EC4 [22], it is shown that the predictions were improved for both square and rectangular sections by P_u/P_{EC*}, safer with less scattered predictions for all the concrete strengths as the effective cross-section areas were used for those slender sections; the predictions also became safer with less scattered predictions by $P_u/P_{EC\wedge}$, when the effective strengths were considered for the infilled concrete strengths of 80 and 120 MPa. However, when considering both effective cross-section area and effective concrete strengths in the calculation for $P_u/P_{EC*\wedge}$, the mean values generally became similar for the different infilled concrete strengths (e.g., mean values of 1.17, 1.16 and 1.16 for infilled concrete of C40, C80 and C120, respectively), which means the effects due to infilled concrete strengths and section slenderness were minimized, as reflected in Figure 13(d) and Figure 14(d). One the contrary, the predictions by the AISC [23], did not show an obvious improvement when the effects due to infilled concrete strengths and section slenderness were taken into consideration, as illustrated in Table 12 and Figures 15-16. For both predictions by EC4 [22] and AISC [23], the predictions were generally more conservative for the lower infilled concrete strengths with less slender sections (non-slender sections), shown in Figures 13(a) and 14(a) for EC4 [22], or more compact sections, shown in Figures 15(a) and 16(a) for AISC [23]. However, the predictions became more conservative (safer) for the higher infilled concrete strengths with more slenderer sections for both EC4 [22] and AISC [23], as shown in Figures 13(a), 14(a), 15(a) and 16(a).

7. Conclusions

The structural behaviour of high strength steel square and rectangular tubular stub columns infilled with concrete has been investigated in the present study. A series of tests was conducted on cold-formed high strength steel (CFHSS) square (ranged from 80×80 mm to 160×160 mm) and rectangular (100×50 mm) tubes infilled with three different grades of concrete (i.e., 40, 80 and 120 MPa). The CFHSS tubular sections had the nominal 0.2% proof stress (i.e. the yield stress) up to 900 MPa. A total of 34 test specimens were designed and tested by applying uniform axial compressive loading. An extensive numerical study accounting for the confinement effect, as well as the non-linearities of materials, geometry and contacts have also been performed by using a validated finite element model.

The behaviour of CFHSS square and rectangular stub columns has been investigated, including the compressive capacities, the end shortening, the strength enhancement index (***SI***) and the ductility index (***DI***). The results showed that the ultimate loads of the CFHSS tubular specimens were significantly improved up to 326% by the infilled concrete in this study. Both the capacities and ductility of the CFHSS square and rectangular stub columns could be significantly enhanced by the infilled concrete. Furthermore, the experimental and numerical results were used to assess the suitability of the design equations specified American Specification (AISC) and European Code (EC4) for the cross-section strength of CFHSS stub columns. Overall, the predictions from EC4 were generally unconservative while the predictions from AISC were conservative. In particular, the predictions were more conservative for the lower infilled concrete strengths with less slender sections (non-slender sections) using EC4 and more compact sections using AISC; however, the predictions became more conservative for the higher infilled concrete strengths with more slenderer sections.

Acknowledgments

The authors would like to thank the technicians in the Structural Engineering Laboratory at The University of Hong Kong for helping the test program.

References

[1] Z. Lai, Z. Huang, and A. H. Varma. Seismic analysis and performance of high strength composite special moment frames (C-SMFs). Structures. 9 (2017), 165–178.
[2] W. Huang, Z. Lai, B. Chen, Z. Xie and A. H. Varma. Concrete-filled steel tube (CFT) truss girders: Experimental tests, analysis, and design. Eng. Struct. 156 (2018), 118–129.
[3] Z. Lai and A. H. Varma. Seismic behavior and modeling of circular concrete partially filled spirally welded pipes (CPFSWP). Thin-Walled Struct. 113 (2017), 240–252.
[4] B. Chen, Z. Lai, Q. Yan, A. H. Varma and X. Yu. Experimental behavior and design of CFT-RC short columns subjected to concentric axial loading. J. Struct. Eng. 2017, 04017148.
[5] F. C. Wang, L. H. Han, and W. Li, Analytical behavior of CFDST stub columns with external stainless steel tubes under axial compression.” Thin Walled Struct. 127 (2018) 756–768.

[6] F. C. Wang, and L. H. Han, Analytical behavior of carbon steel-concrete stainless steel double-skin tube (DST) used in submarine pipeline structure, Mar. Struct. 63 (2019) 99–116.
[7] L. H. Han, Concrete-filled steel tubes structure-theory to practice. [In Chinese.]. Beijing: Science Press. 2007.
[8] F.-X. Ding, W.-J. Wang, D.-R. Lua and X.-M. Liu. Study on the behavior of concrete-filled square double-skin steel tubular stub columns under axial loading. Structures 23 (2020) 665–676.
[9] J.Y. Richard Liew, Mingxiang Xiong and Dexin Xiong. Design of Concrete Filled Tubular Beam-columns with High Strength Steel and Concrete, Structures, 8 (2), (2016) 213-226.
[10] I. Nishiyama, S. Morino, K. Sakino, *et al.* Summary of research on concrete-filled structural steel tube column system carried out under the US-Japan cooperative research on composite and hybrid structures. Ibaraki Prefecture, Japan: Building Research Institute, 2002.
[11] D. K. Kim, A database for composite columns." M.S. thesis, School of Civil and Environmental Engineering, Georgia Institute of Technology, 2005.
[12] C. D. Goode, Composite columns—1819 tests on concrete-filled steel tube columns compared with Eurocode 4, Struct. Eng. 86 (16) (2008) 33–38.
[13] L. H. Han, W. Li, and R. Bjorhovde, Developments and advanced applications of concrete-filled steel tubular (CFST)structures: Members, J. Constr. Steel Res. 100 (2014) 211–228.
[14] Son Thai, H.-T. Thai, B. Uy and T. Ngo, Concrete-filled steel tubular columns: Test database, design and calibration, J. Constr. Steel Res. 157 (2019) 161-181.
[15] J. F., Hajjar, B. C. Gourley, C. Tort, M. D. Denavit, P. H. Schiller, and N. Leipziger Mundis, Steel-Concrete Composite Structural Systems, Department of Civil and Environmental Engineering, Northeastern University, Boston, Massachusetts, 2019, <http://www.northeastern.edu/compositesystems>.
[16] Lai, Z., and Varma, A. H. High-Strength Rectangular CFT Members: Database, Modeling, and Design of Short Columns. J. Struct. Eng., 2018, 04018036.
[17] J. Wei, X. Luo; Z. Lai, and A. H. Varma, Experimental Behavior and Design of High-Strength Circular Concrete-Filled Steel Tube Short Columns, J. Struct. Eng. 146(1) (2019): 04019184.
[18] J.-L. Ma, T.-M. Chan and B. Young, Material properties and residual stresses of cold-formed high strength steel hollow sections, J. Constr. Steel Res.,109 (2015) 152-165.
[19] M. X. Xiong, D. X. Xiong and J. Y. R. Liew, Axial performance of short concrete filled steel tubes with high- and ultra-high-strength materials, Eng. Struct. 136 (2017) 494–510.
[20] K. Sakino, H. Nakahara, S. Morino, and A. Nishiyama, Behaviorof centrally loaded concrete-filled steel-tube short columns, J. Struct. Eng. 130 (2) (2004) 180-188.
[21] M. Khan, B. Uy, Z. Tao, F. Mashiri,Behaviour and design of short high-strength steel welded box and concrete-filled tube (CFT) sections, Eng. Struct. 147 (2017) 458–472.
[22] EC4. Eurocode 4: Design of composite steel and concrete structures. 1-1: General rules and rules for buildings control. European Committee for Standardization (CEN) EN 1994-1-1. Brussels, Belgium: CEN, 2004.
[23] AISC. Specification for structural steel buildings. AISC 360. Chicago: AISC 2016.
[24] AIJ. Recommendations for design and construction of concrete filled steel tubular structures. Architectural Institute of Japan (AIJ), Tokyo, 2008.

671 [25] AS/NZS2327, Composite structures - Composite steel-concrete construction in buildings,
672 Australian/New Zealand Standard, 2017.
673 [26] ACI, Building Code Requirements for Structural Concrete (ACI 318M-14) and Commentary
674 (ACI 318RM-14), American Concrete Institute, Detroit, USA, 2014.
675 [27] M. Su, Y. Cai, X. Chen and B. Young. Behaviour of concrete-filled cold-formed high strength
676 steel circular stub columns. Thin-Walled Structures, 157 (2020) 107078.
677 [28] Y. Cai, W.M. Quach and B. Young, Experimental and numerical investigation of concrete-filled
678 hot-finished and cold-formed steel elliptical tubular stub columns, Thin-Walled Structures, 145 (2019)
679 106437.
680 [29] ABAQUS Analysis User's Manual, ABAQUS, Inc., 2017, Version 6.14.
681 [30] X. Dai, D. Lam, Numerical modelling of the axial compressive behavior of short concrete-filled
682 elliptical steel columns, J. Constr. Steel Res. 66 (7) (2010) 931–942.
683 [31] Thai Huu-Tai, Uy Brian, Khan Mahbub, Tao Zhong, Mashiri Fidelis. Numerical modelling of
684 concrete-filled steel box columns incorporating high strength materials. Journal of Constructional
685 Steel Research 102 (2014) 256–265.
686 [32] Lam D, X. H. Dai, L.H. Han Q. X. Ren and W. Li, Behaviour of inclined, tapered and STS square
687 CFST stub columns subjected to axial load, Thin-Walled Structure, 54 (2012) 94–105.
688 [33] Al-Ani Yahia Raad. Finite element study to address the axial capacity of the circular concrete-
689 filled steel tubular stub columns. Thin-Walled Structures 126 (2018) 2-15.
690 [34] J.-L. Ma, T.-M. Chan and B. Young, Design of Cold-Formed High-Strength Steel Tubular Stub
691 Columns, J. Struct. Eng., 144(6) (2018) 04018063.
692 [35] Z. Tao, B. Uy, F.-Y. Liao and L.-H. Han, Nonlinear analysis of concrete-filled square stainless
693 steel stub columns under axial compression, J. Constr. Steel Res. 67 (2011) 1719–1732.
694 [36] Z. Tao, B. Uy, L.-H. Han and Z.-B. Wang, Analysis and design of concrete-filled stiffened thin-
695 walled steel tubular columns under axial compression, Thin-Walled Struct. 47 (2009) 1544–1556.
696 [37] L.H. Han, G.H. Yao and Z. Tao, Performance of concrete-filled thin-walled steel tubes
697 under pure torsion, Thin-Walled Struct, 45(1) (2007) 24–36.
698 [38] Z. Tao, Z. B. Wang and Q. Yu, Finite element modelling of concrete-filled steel stub columns
699 under axial compression, Journal of Constructional Steel Research. 89 (2013) 121–131.
700 [39] V. K. Papanikolaou and A. J. Kappos, Confinement-sensitive plasticity constitutive model for
701 concrete in triaxial compression, International Journal of Solids and Structures, 44(21) (2007) 7021-
702 7048
703 [40] T. Yu, J.G. Teng, Y.L. Wong, and S.L. Dong, Finite element modeling of confined concrete-I:
704 Drucker–Prager type plasticity model, Engineering Structures. 32(3) (2010) 665-679
705 [41] FIP. CEB-FIP Model Code 1990. London: Thomas Telford Ltd.; 1993.
706 [42] Z.P. Bažant, E. Becq-Giraudon. Statistical prediction of fracture parameters of concrete and
707 implications for choice of testing standard. Cem Concr Res. 32(4) (2002) 529–56.
708 [43] F. Wang, B. Young, L. Gardner, Compressive testing and numerical modelling of concrete-filled
709 double skin CHS with austenitic stainless steel outer tubes, Thin-Walled Struct. 141 (2019) 345–359
710 [44] EC3-1.5. Eurocode 3: Design of steel structures - Part 1-5: Plated structural elements. CEN
711 (European Committee for Standardization). EN 1993-1-5. Brussels, Belgium: CEN, 2006.
712

Table 1: Material properties of CFHSS square and rectangular tubes

Tube labelling	E_s (GPa)	$f_{0.2}$ (MPa)	f_u (MPa)	ε_u (%)	ε_f (%)
80×80×4-A	211	756	852	3.0	16.0
100×50×4-A	212	721	842	4.3	14.7
100×100×4-A	215	722	819	5.7	18.0
140×140×5-A	210	682	822	6.4	21.0
160×160×4-A	215	629	881	3.8	13.4
80×80×4-B	210	1022	1179	1.9	11.8
100×100×4-B	206	980	1092	1.7	12.1
120×120×4-B	206	991	1140	2.9	12.2

Table 2: Compressive strength (f_{ck}) of concrete cylinders

Concrete mixes	28 days (MPa)	Column test day (MPa)
C40	34.9	35.5
C80	79.9	85.7
C120	112.7	114.9

Note: data source from Ref. [27].

Table 3: Dimensions of high strength steel tubes of Series A

Specimens	H (mm)	B (mm)	r_i (mm)	t (mm)	L (mm)
80×80×4-C0-A	80.6	80.2	5.0	4.00	240.0
80×80×4-C40-A	80.1	80.4	4.9	4.00	240.0
80×80×4-C80-A	80.5	80.2	5.0	3.98	240.0
80×80×4-C120-A	80.7	80.2	5.0	3.96	240.0
100×50×4-C0-A	100.2	50.9	3.5	3.97	300.0
100×50×4-C40-A	100.2	50.6	3.4	3.98	300.0
100×50×4-C40-A-r	100.2	50.7	3.5	3.96	300.0
100×50×4-C80-A	100.2	50.9	3.5	4.00	300.0
100×50×4-C120-A	100.3	50.8	3.6	3.96	299.0
100×100×4-C0-A	100.6	100.8	4.3	4.00	300.0
100×100×4-C40-A	100.4	100.7	4.2	3.99	300.0
100×100×4-C80-A	100.9	100.6	4.3	3.97	300.0
100×100×4-C120-A	100.8	100.5	4.3	3.96	299.5
140×140×5-C0-A	140.8	141.7	7.0	4.91	420.0
140×140×5-C40-A	141.2	140.7	7.0	4.94	420.0
140×140×5-C80-A	141.0	141.4	7.1	4.97	420.0
140×140×5-C120-A	141.4	141.1	7.0	4.93	420.0
160×160×4-C0-A	161.8	161.1	6.0	4.05	480.0
160×160×4-C40-A	161.2	161.7	6.0	4.01	480.0
160×160×4-C80-A	161.5	161.9	6.0	4.01	480.0
160×160×4-C120-A	162.0	161.2	6.0	4.04	480.0

Table 4: Dimensions of high strength steel tubes of Series B

Specimens	H (mm)	B (mm)	r_i (mm)	t (mm)	L (mm)
80×80×4-C0-B	80.5	80.3	6.0	3.98	239.0
80×80×4-C40-B	80.3	80.5	6.1	3.97	240.0
80×80×4-C80-B	80.5	80.2	5.8	3.99	240.0
80×80×4-C120-B	80.4	80.3	6.0	3.98	240.0
100×100×4-C0-B	100.6	100.7	7.0	4.01	300.0
100×100×4-C40-B	100.6	100.6	7.0	4.00	299.5
100×100×4-C80-B	100.9	100.6	7.0	3.97	299.5
100×100×4-C120-B	100.7	100.7	7.0	3.99	299.5
120×120×4-C0-B	121.8	121.6	6.0	3.93	360.0
120×120×4-C40-B	121.9	121.8	6.0	3.93	360.0
120×120×4-C80-B	121.8	121.8	6.0	3.91	359.0
120×120×4-C80-B-r	121.9	121.8	6.0	3.93	359.0
120×120×4-C120-B	121.9	121.9	6.0	3.92	360.0

Table 5: Test results of concrete-filled CFHSS stub columns using Series A steel tubes

Specimens	*H/B*	*h/t*	P_t (kN)	δ_u (mm)	$\delta_{0.85u}$ (mm)	*Nor.*	*DI*
80×80×4-C0-A	1.0	15.7	1064	3.2	4.0	1.00	1.25
80×80×4-C40-A	1.0	15.6	1328	3.3	5.4	1.25	1.64
80×80×4-C80-A	1.0	15.7	1462	3.3	>9.8	1.37	>2.97
80×80×4-C120-A	1.0	15.8	1504	3.4	6.5	1.41	1.91
100×50×4-C0-A	2.0	21.5	922	2.8	3.9	1.00	1.39
100×50×4-C40-A	2.0	21.5	1113	3.0	4.6	1.21	1.53
100×50×4-C40-A-r	2.0	21.5	1112	5.1	6.0	1.21	1.18
100×50×4-C80-A	2.0	21.3	1211	4.0	6.0	1.31	1.50
100×50×4-C120-A	2.0	21.5	1198	3.4	5.1	1.30	1.50
100×100×4-C0-A	1.0	21.0	1241	2.3	2.8	1.00	1.22
100×100×4-C40-A	1.0	21.0	1666	3.0	>4.7	1.34	>1.57
100×100×4-C80-A	1.0	21.3	1853	2.8	5.1	1.49	1.82
100×100×4-C120-A	1.0	21.3	1957	2.9	>8.2	1.58	>2.83
140×140×5-C0-A	1.0	23.8	2033	2.6	3.2	1.00	1.23
140×140×5-C40-A	1.0	23.7	2992	5.2	15.1	1.47	2.90
140×140×5-C80-A	1.0	23.5	3237	4.3	13.3	1.59	3.09
140×140×5-C120-A	1.0	23.8	3760	2.6	5.0	1.85	1.92
160×160×4-C0-A	1.0	35.0	1246	1.7	3.6	1.00	2.12
160×160×4-C40-A	1.0	35.2	2785	3.9	>6.4	2.24	>1.64
160×160×4-C80-A	1.0	35.3	3600	2.3	4.7	2.89	2.04
160×160×4-C120-A	1.0	35.1	4062	2.1	3.9	3.26	1.86

Note: "*Nor.*" represents the P_t normalized by that ($P_{t,0}$) without infilled concrete in the same series.

Table 6: Test results of concrete-filled CFHSS stub columns using Series B steel tubes

Specimens	*H/B*	*h/t*	P_t (kN)	δ_u (mm)	$\delta_{0.85u}$ (mm)	*Nor.*	*DI*
80×80×4-C0-B	1.0	15.2	1431	3.3	3.8	1.00	1.15
80×80×4-C40-B	1.0	15.1	1722	3.4	4.6	1.20	1.35
80×80×4-C80-B	1.0	15.3	1791	3.7	7.5	1.25	2.03
80×80×4-C120-B	1.0	15.2	1898	3.4	5.9	1.33	1.74
100×100×4-C0-B	1.0	19.6	1474	2.8	3.2	1.00	1.14
100×100×4-C40-B	1.0	19.7	2009	4.7	7.2	1.36	1.53
100×100×4-C80-B	1.0	19.9	2177	4.1	7.1	1.48	1.73
100×100×4-C120-B	1.0	19.7	2266	4.3	>9.3	1.54	>2.16
120×120×4-C0-B	1.0	25.9	1400	1.9	3.3	1.00	1.74
120×120×4-C40-B	1.0	26.0	2557	4.1	5.5	1.83	1.34
120×120×4-C80-B	1.0	26.1	2853	4.2	>11.7	2.04	>2.79
120×120×4-C80-B-r	1.0	26.0	2798	3.3	>11.6	2.00	>3.52
120×120×4-C120-B	1.0	26.0	2950	2.9	>11.0	2.11	>3.79

Table 7: Comparison of test strengths with FE predictions

Specimens	P_t (kN)	P_{FEA} (kN)	P_t/P_{FEA}
80×80×4-C0-A	1064	1039	1.02
80×80×4-C40-A	1328	1242	1.07
80×80×4-C80-A	1462	1418	1.03
80×80×4-C120-A	1504	1513	0.99
100×50×4-C0-A	922	902	1.02
100×50×4-C40-A	1113	1129	0.99
100×50×4-C80-A	1211	1250	0.97
100×50×4-C120-A	1193	1360	0.88
100×100×4-C0-A	1241	1205	1.03
100×100×4-C40-A	1666	1580	1.05
100×100×4-C80-A	1853	1825	1.02
100×100×4-C120-A	1957	2076	0.94
140×140×5-C0-A	2033	2134	0.95
140×140×5-C40-A	2992	3028	0.99
140×140×5-C80-A	3237	3321	0.97
140×140×5-C120-A	3760	3735	1.01
160×160×4-C0-A	1246	1225	1.02
160×160×4-C40-A	2785	2257	1.23
160×160×4-C80-A	3600	3198	1.13
160×160×4-C120-A	4062	4226	0.96
80×80×4-C0-B	1431	1377	1.04
80×80×4-C40-B	1722	1637	1.05
80×80×4-C80-B	1791	1728	1.04
80×80×4-C120-B	1898	1797	1.06
100×100×4-C0-B	1474	1639	0.90
100×100×4-C40-B	2009	2006	1.00
100×100×4-C80-B	2177	2214	0.98
100×100×4-C120-B	2266	2387	0.95
120×120×4-C0-B	1400	1874	0.75
120×120×4-C40-B	2557	2606	0.98
120×120×4-C80-B	2853	2864	1.00
120×120×4-C120-B	2950	3085	0.96
		Mean	1.00
		COV	0.079

Table 8: Dimensions and results of concrete-filled CFHSS square stub columns in parametric study

Specimens	*h*/*t*	P_{FEA} (kN)	δ_u (mm)	$\delta_{0.85u}$ (mm)	*Nor.*	*DI*
45×45×3-C0-A	10.0	408	1.93	2.88	1.00	1.49
45×45×3-C40-A		499	8.62	-	1.22	
45×45×3-C80-A		529	4.31	13.36	1.30	3.10
45×45×3-C120-A		567	5.05	8.98	1.39	1.78
250×250×5-C0-A	45.0	2310	3.75	8.55	1.00	2.28
250×250×5-C40-A		4603	1.88	4.07	1.99	2.16
250×250×5-C80-A		7050	2.05	2.69	3.05	1.31
250×250×5-C120-A		9650	2.45	2.93	4.18	1.20
360×360×6-C0-A	55.0	4543	3.33	10.63	1.00	3.19
360×360×6-C40-A		8690	2.67	4.42	1.91	1.66
360×360×6-C80-A		13994	2.96	3.64	3.08	1.23
360×360×6-C120-A		19071	3.32	4.10	4.20	1.23
45×45×3-C0-B	10.0	545	1.55	1.96	1.00	1.26
45×45×3-C40-B		641	1.93	-	1.18	
45×45×3-C80-B		663	2.00	2.91	1.22	1.46
45×45×3-C120-B		682	1.77	2.85	1.25	1.61
160×160×4-C0-B	35.0	1437	2.34	4.26	1.00	1.82
160×160×4-C40-B		2182	1.83	2.06	1.52	1.13
160×160×4-C80-B		3428	1.59	2.97	2.39	1.87
160×160×4-C120-B		4460	1.76	2.42	3.10	1.38
250×250×5-C0-B	45.0	2718	4.80	7.89	1.00	1.64
250×250×5-C40-B		5089	4.01	7.12	1.87	1.78
250×250×5-C80-B		7410	2.34	3.62	2.73	1.55
250×250×5-C120-B		10125	2.59	3.22	3.73	1.24
360×360×6-C0-B	55.0	5093	3.42	3.56	1.00	1.04
360×360×6-C40-B		8996	2.74	10.74	1.77	3.92
360×360×6-C80-B		14406	3.09	4.03	2.83	1.30
360×360×6-C120-B		19615	3.20	3.89	3.85	1.22

Note: "*Nor.*" represents the P_{FEA} normalized by that ($P_{FEA,0}$) without infilled concrete in the same series.

Table 9: Dimensions and results of concrete-filled CFHSS rectangular stub columns in parametric study

Specimens	*h*/*t*	P_{FEA} (kN)	δ_u (mm)	$\delta_{0.85u}$ (mm)	*Nor.*	*DI*
120×60×3-C0-A	35.0	659	1.82	3.64	1.00	2.00
120×60×3-C40-A		912	1.98	3.99	1.38	2.02
120×60×3-C80-A		1096	1.23	2.25	1.66	1.83
120×60×3-C120-A		1382	1.30	1.54	2.10	1.18
180×90×3-C0-A	55.0	759	2.23	4.10	1.00	1.84
180×90×3-C40-A		1550	1.46	2.90	2.04	1.99
180×90×3-C80-A		2044	1.72	1.94	2.69	1.13
180×90×3-C120-A		2673	1.95	2.17	3.52	1.11
320×160×4-C0-A	75.0	1829	5.53	11.64	1.00	2.10
320×160×4-C40-A		3595	2.55	2.83	1.97	1.11
320×160×4-C80-A		5619	2.91	3.18	3.07	1.09
320×160×4-C120-A		7586	3.10	4.24	4.15	1.37
120×60×3-C0-B	35.0	807	2.46	3.33	1.00	1.35
120×60×3-C40-B		1128	2.38	3.37	1.40	1.42
120×60×3-C80-B		1232	2.08	3.14	1.53	1.51
120×60×3-C120-B		1468	1.33	2.33	1.82	1.75
180×90×3-C0-B	55.0	920	2.99	4.19	1.00	1.40
180×90×3-C40-B		1543	1.74	3.41	1.68	1.96
180×90×3-C80-B		2182	1.83	2.06	2.37	1.13
180×90×3-C120-B		2781	1.98	2.23	3.02	1.13
320×160×4-C0-B	75.0	2142	6.41	9.83	1.00	1.53
320×160×4-C40-B		3778	2.65	6.47	1.76	2.44
320×160×4-C80-B		5805	2.94	3.25	2.71	1.11
320×160×4-C120-B		7652	3.34	3.69	3.57	1.10

Note: "*Nor.*" represents the P_{FEA} normalized by that ($P_{FEA,0}$) without infilled concrete in the same series.

Table 10: Comparison of test and FE results with predictions from EC4 [22]

Specimens	No.			P_u/P_{EC}	P_u/P_{EC*}	$P_u/P_{EC\wedge}$	$P_u/P_{EC*\wedge}$
Square specimens	21	Series A	Mean	1.03	1.10	1.09	1.18
			COV	0.137	0.096	0.115	0.074
	22	Series B	Mean	0.95	1.08	1.01	1.15
			COV	0.180	0.097	0.167	0.091
	43	Series A&B	Mean	0.99	1.09	1.05	1.17
			COV	0.162	0.096	0.147	0.083
Rectangular specimens	13	Series A	Mean	0.96	1.09	1.02	1.16
			COV	0.127	0.064	0.115	0.063
	9	Series B	Mean	0.81	1.05	0.86	1.13
			COV	0.084	0.041	0.109	0.065
	22	Series A&B	Mean	0.90	1.07	0.95	1.15
			COV	0.141	0.059	0.138	0.064

Note: P_{EC*} = modified predicted strength incorporating effective area of steel tube; $P_{EC\wedge}$ = modified predicted strength incorporating the effective compressive strength of concrete; and $P_{EC*\wedge}$ = modified predicted strength incorporating both the effective area of steel tube and effective compressive strength of concrete.

Table 11: Comparison of test and FE results with predictions from AISC [23]

Specimens	No.			P_u/P_{AISC}	$P_u/P_{AISC\wedge}$
Square specimens	21	Series A	Mean	1.12	1.19
			COV	0.101	0.097
	22	Series B	Mean	1.07	1.12
			COV	0.140	0.147
	43	Series A&B	Mean	1.09	1.16
			COV	0.123	0.126
Rectangular specimens	13	Series A	Mean	1.17	1.24
			COV	0.142	0.173
	9	Series B	Mean	1.20 (1.30)*	1.29 (1.41)*
			COV	0.209 (0.300)*	0.242(0.325)*
	22	Series A&B	Mean	1.18 (1.22)*	1.26 (1.31)*
			COV	0.170 (0.228)*	0.200 (0.256)*

Note: "(x)*" = modified predicted strength incorporating effective area of steel tube; $P_{AISC\wedge}$ = modified predicted strength incorporating the effective compressive strength of concrete

Table 12: Comparison of test and FE results with codified predictions for specimens with different infilled concrete compressive strengths

(a) Square specimens

Cases		No. of columns	P_u/P_{EC}	P_u/P_{EC*}	$P_u/P_{EC\wedge}$	$P_u/P_{EC*\wedge}$	P_u/P_{AISC}	$P_u/P_{AISC\wedge}$
Infilled concrete C40	Mean	14	1.04	1.17	1.04	1.17	1.12	1.12
	COV		0.232	0.120	0.232	0.120	0.176	0.176
Infilled concrete C80	Mean	15	0.97	1.07	1.05	1.16	1.08	1.15
	COV		0.121	0.050	0.109	0.051	0.088	0.087
Infilled concrete C120	Mean	14	0.96	1.03	1.06	1.16	1.08	1.20
	COV		0.076	0.046	0.060	0.072	0.086	0.102
All cases	Mean	43	0.99	1.09	1.05	1.17	1.09	1.16
	COV		0.162	0.096	0.147	0.083	0.123	0.126

Note: P_{EC*} = modified predicted strength incorporating effective area of steel tube; $P_{EC\wedge}$ = modified predicted strength incorporating the effective compressive strength of concrete; and $P_{EC*\wedge}$ = modified predicted strength incorporating both the effective area of steel tube and effective compressive strength of concrete; $P_{AISC\wedge}$ = modified predicted strength incorporating the effective compressive strength of concrete.

(b) Rectangular specimens

Cases		No. of columns	P_u/P_{EC}	P_u/P_{EC*}	$P_u/P_{EC\wedge}$	$P_u/P_{EC*\wedge}$	P_u/P_{AISC}	$P_u/P_{AISC\wedge}$
Infilled concrete C40	Mean	8	0.92	1.12	0.92	1.12	1.18 (1.24)*	1.18 (1.24)*
	COV		0.211	0.054	0.211	0.054	0.157 (0.256)*	0.157 (0.256)*
Infilled concrete C80	Mean	7	0.88	1.05	0.94	1.14	1.18 (1.21)*	1.27 (1.32)*
	COV		0.106	0.038	0.101	0.056	0.195 (0.245)*	0.220 (0.281)*
Infilled concrete C120	Mean	7	0.89	1.03	1.00	1.18	1.19 (1.21)*	1.35 (1.38)*
	COV		0.061	0.043	0.060	0.076	0.183 (0.211)*	0.221 (0.258)*
All cases	Mean	22	0.90	1.07	0.95	1.15	1.18 (1.22)*	1.26 (1.31)*
	COV		0.141	0.059	0.138	0.064	0.170 (0.228)*	0.200 (0.256)*

Note: "(x)*" result by using reduced cross section area of steel tube.

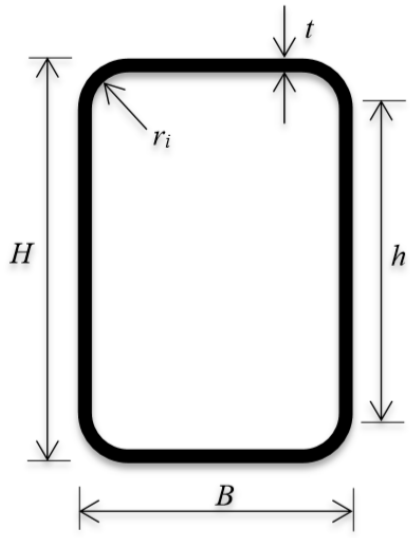

Figure 1: Symbols of CFHSS cross section

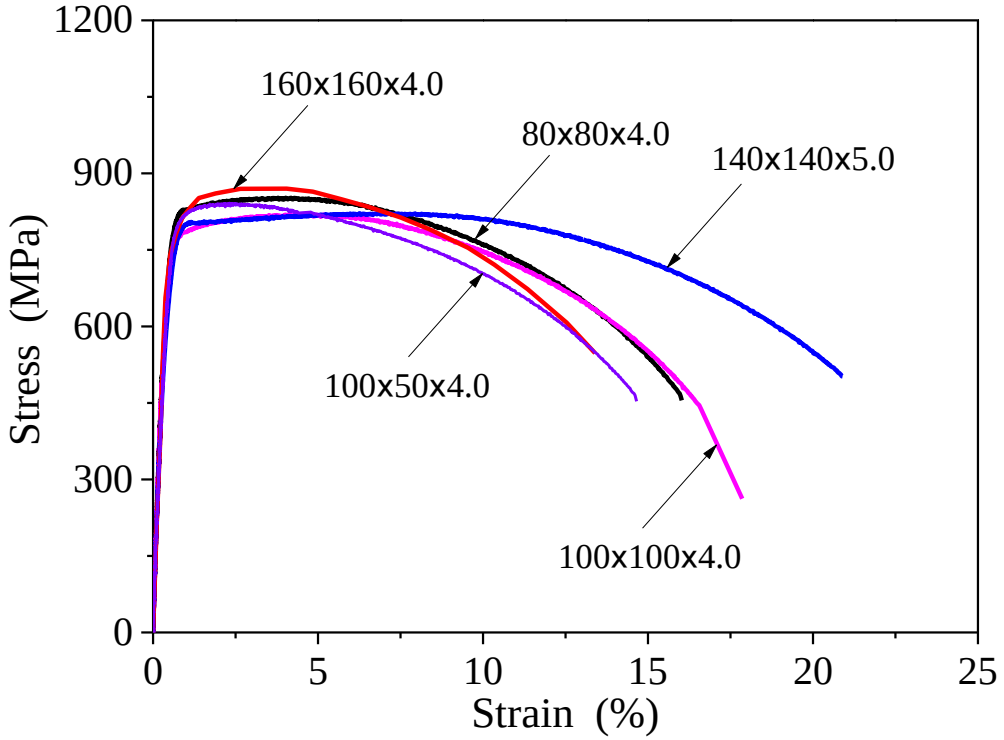

a) Members with nominal 0.2.% proof stress of 700 MPa

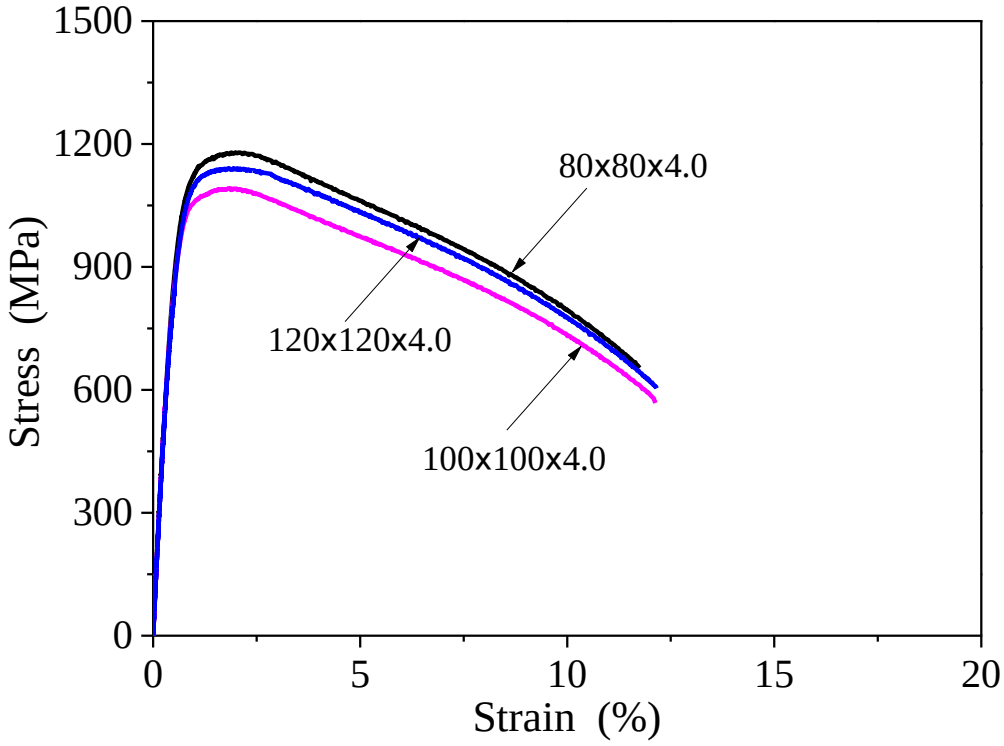

b) Members with nominal 0.2.% proof stress of 900 MPa

Figure 2: Measured stress-strain curves of high strength steel tubular members

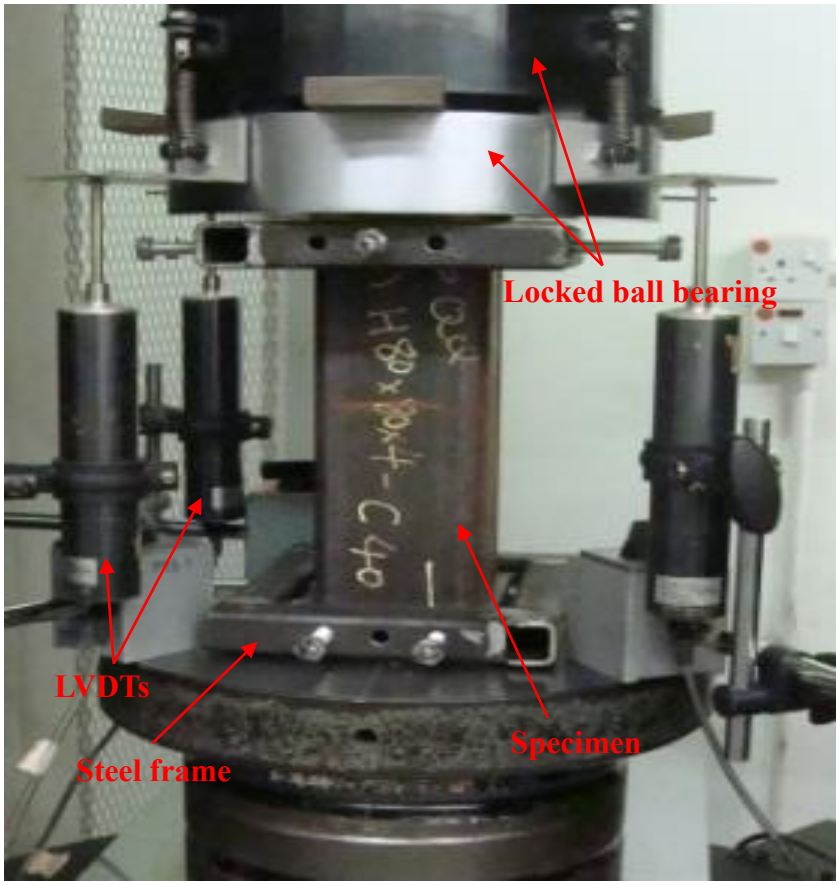

Figure 3: Test setup of concrete-filled stub column Specimen 80×80×4-C40-A

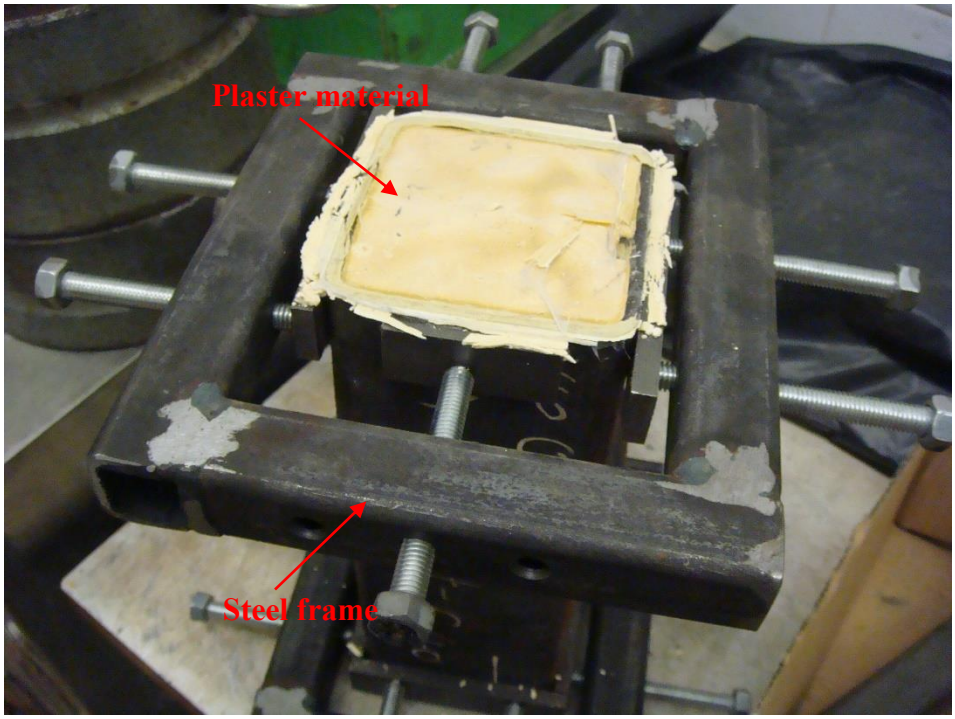

Figure 4: Specimen 80×80×4-C40-A after compressive test

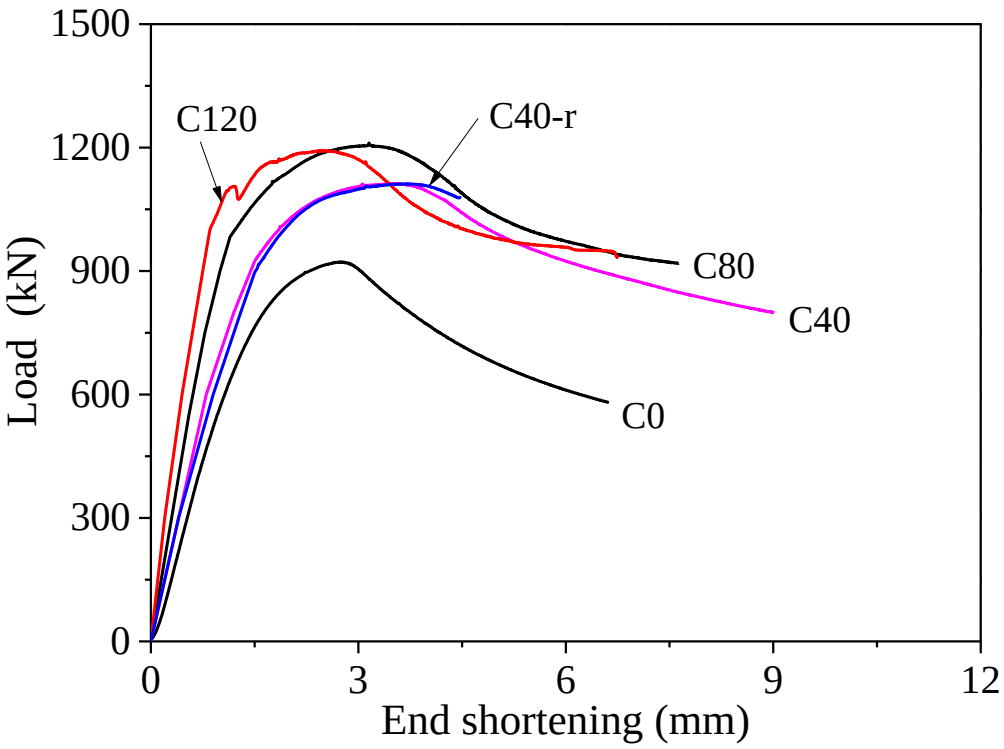

(a) Series 100×50×4-A

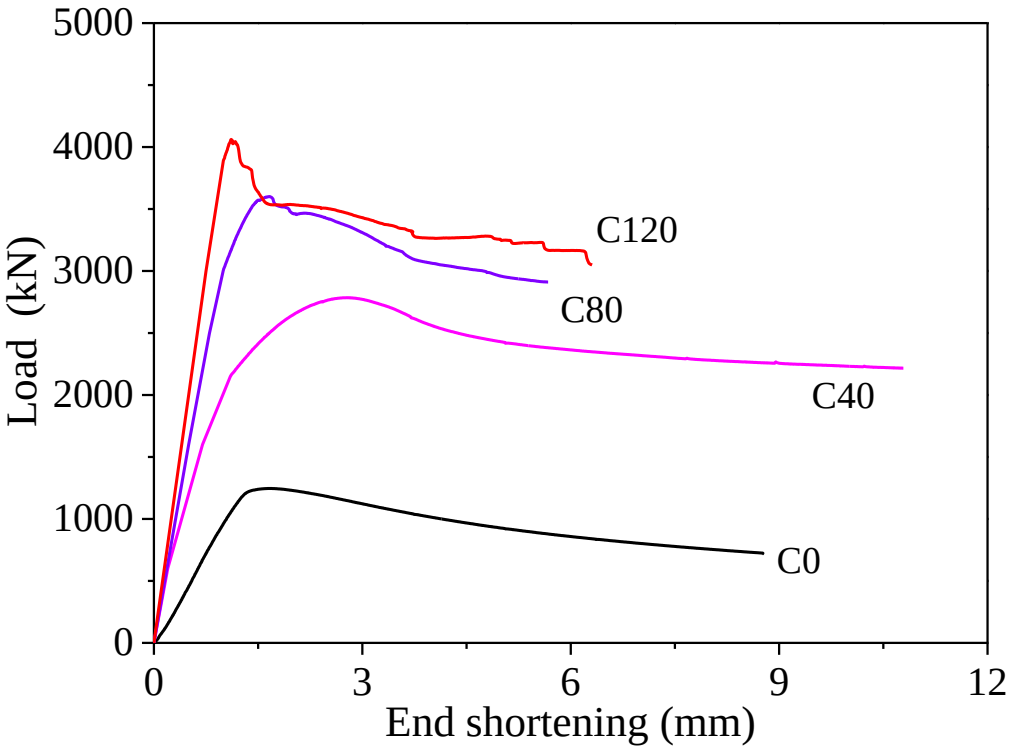

(b) Series 160×160×4-A

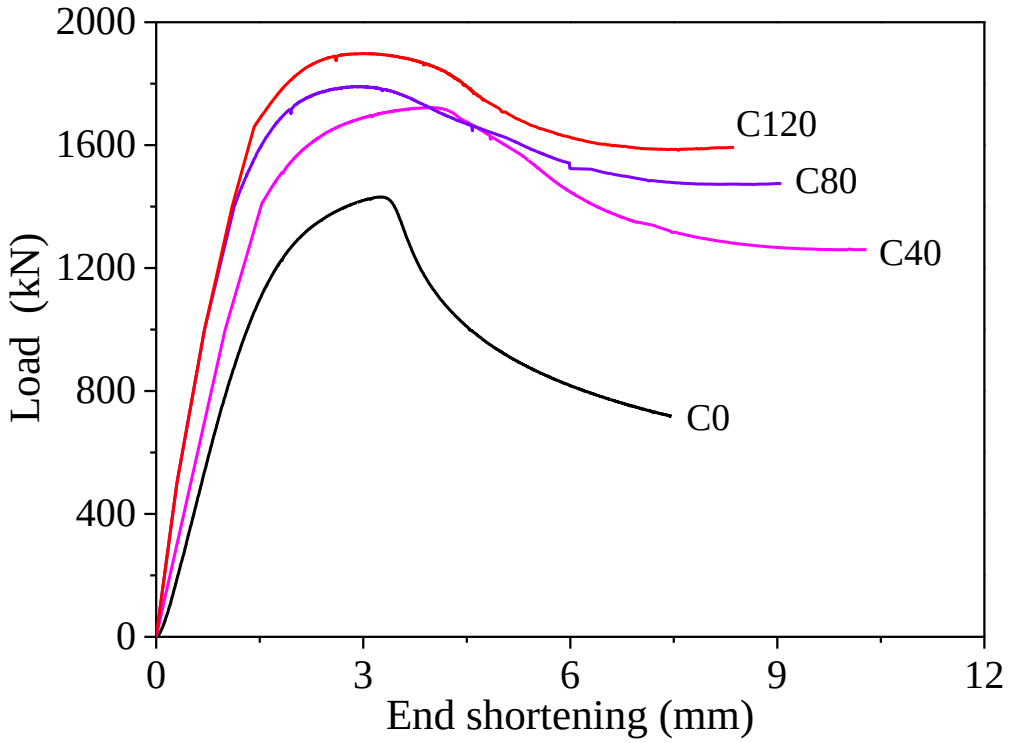

(c) Series 80×80×4-B

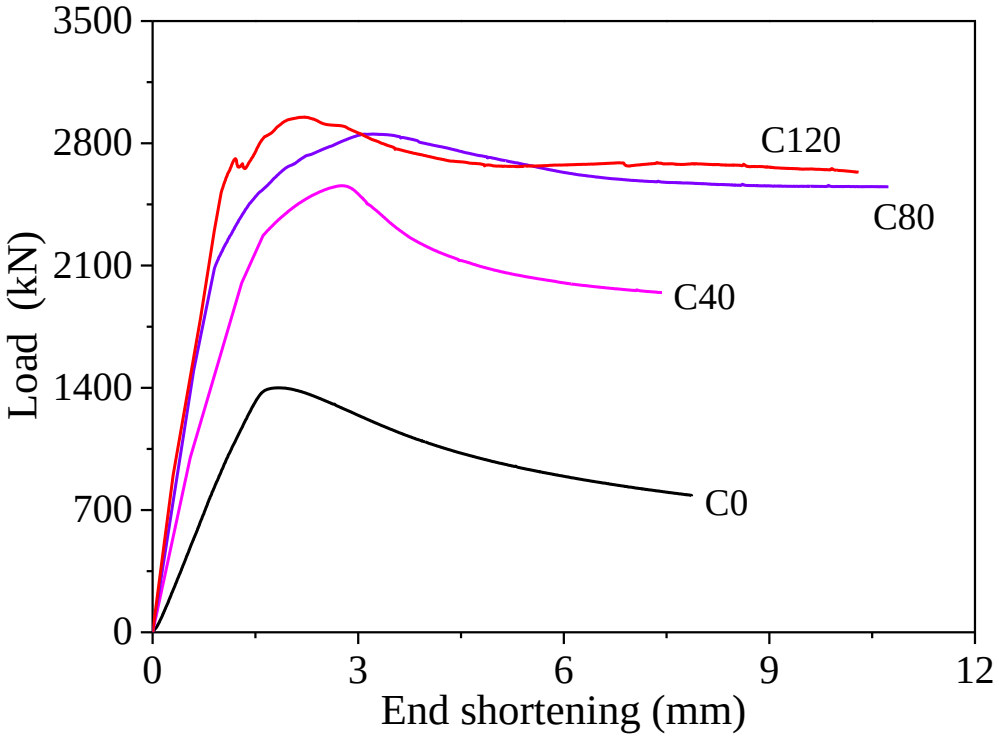

(d) Series 120×120×4-B

Figure 5: Load-end shortening curves of concrete-filled CFHSS stub columns

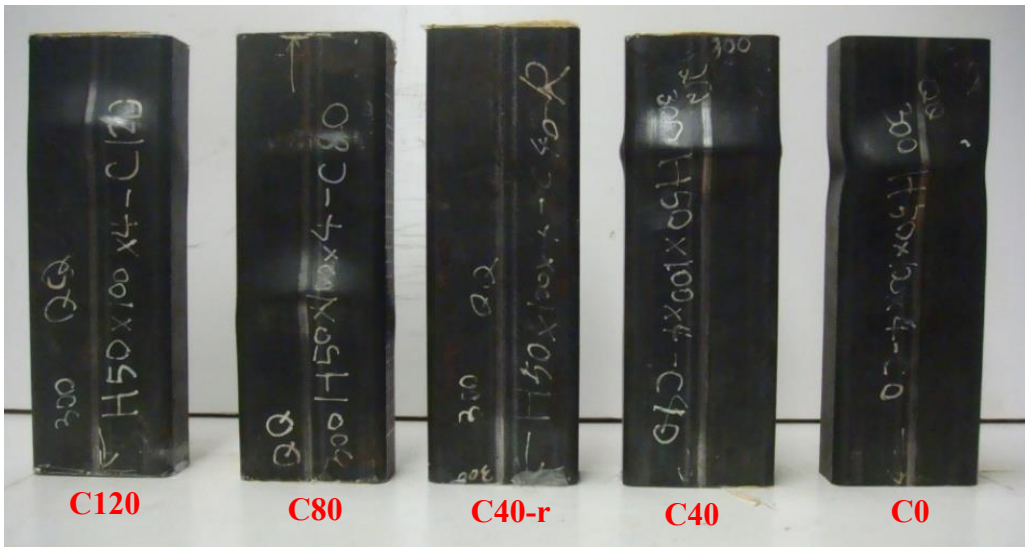

Figure 6: Failure modes of stub columns (series 100×50×4-A)

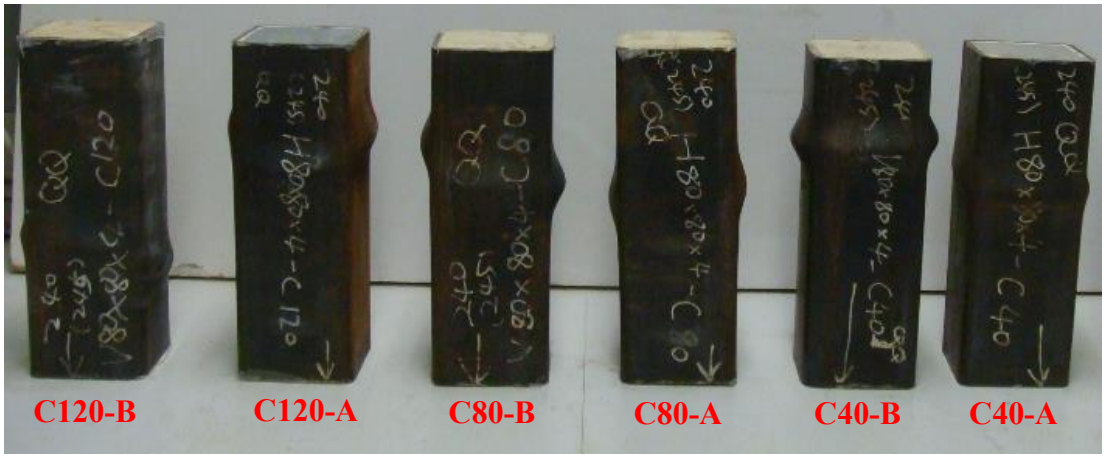

Figure 7: Failure modes of stub columns (series 80×80×4-A and 80×80×4-B)

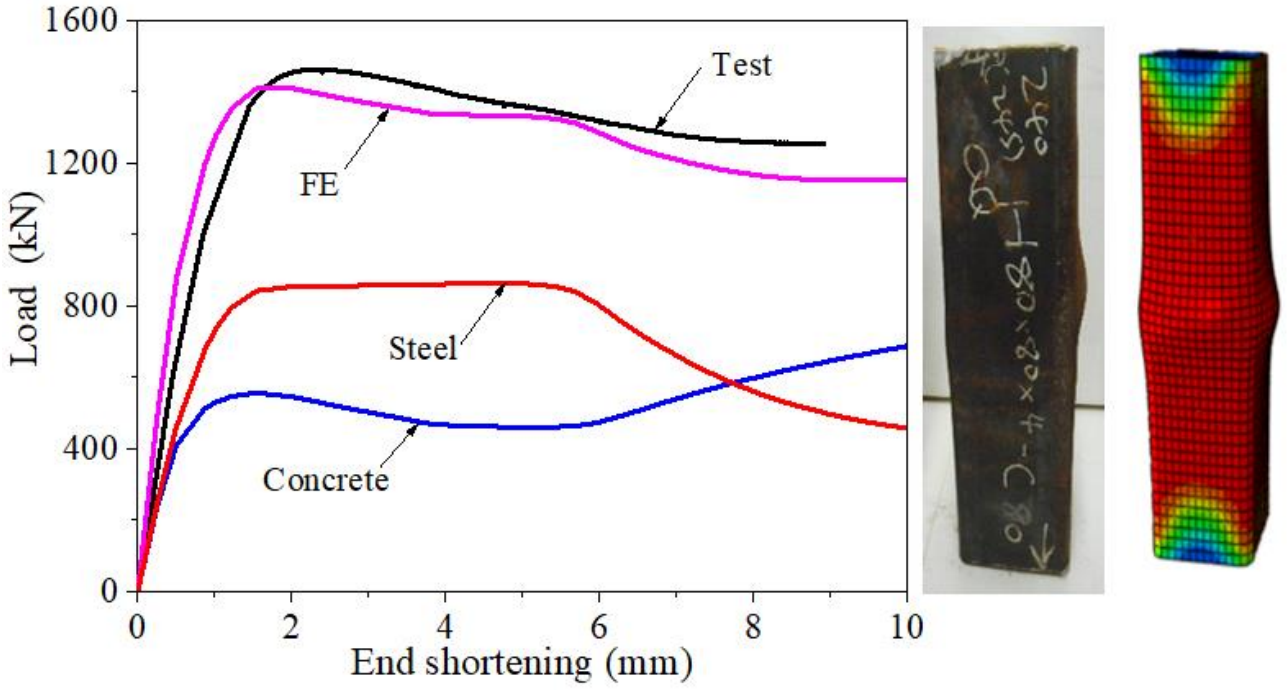

Figure 8: Comparison of test results and numerical predictions for Specimen 80×80×4-C80-A

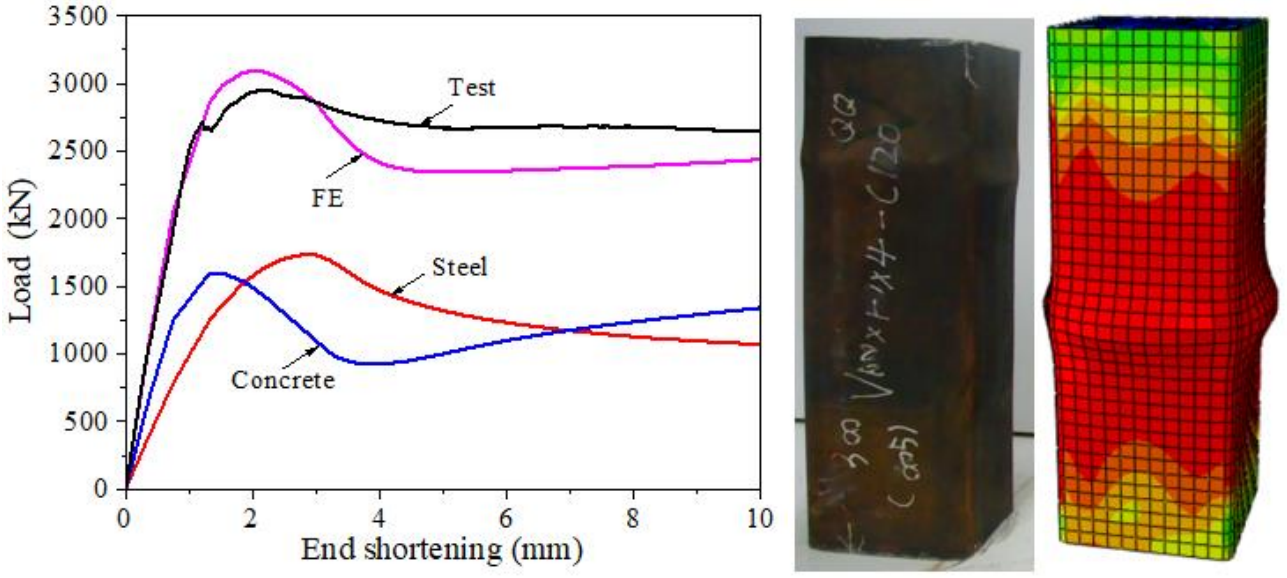

Figure 9: Comparison of test results and numerical predictions for Specimen 120×120×4-C120-B

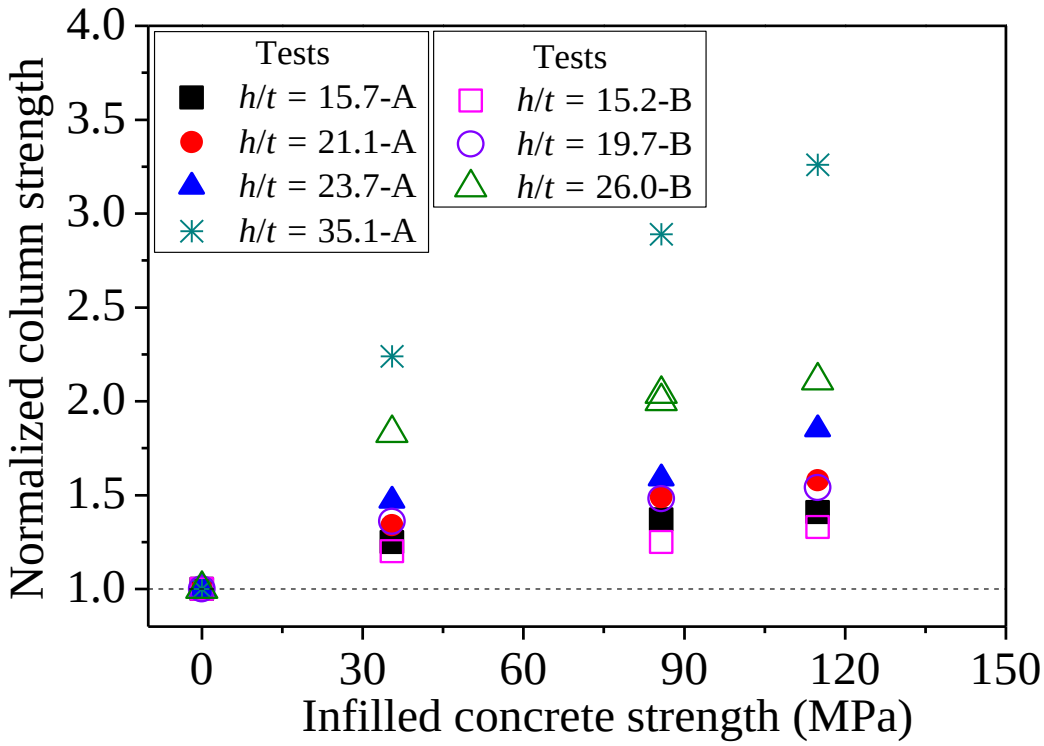

(a) Square sections from test results

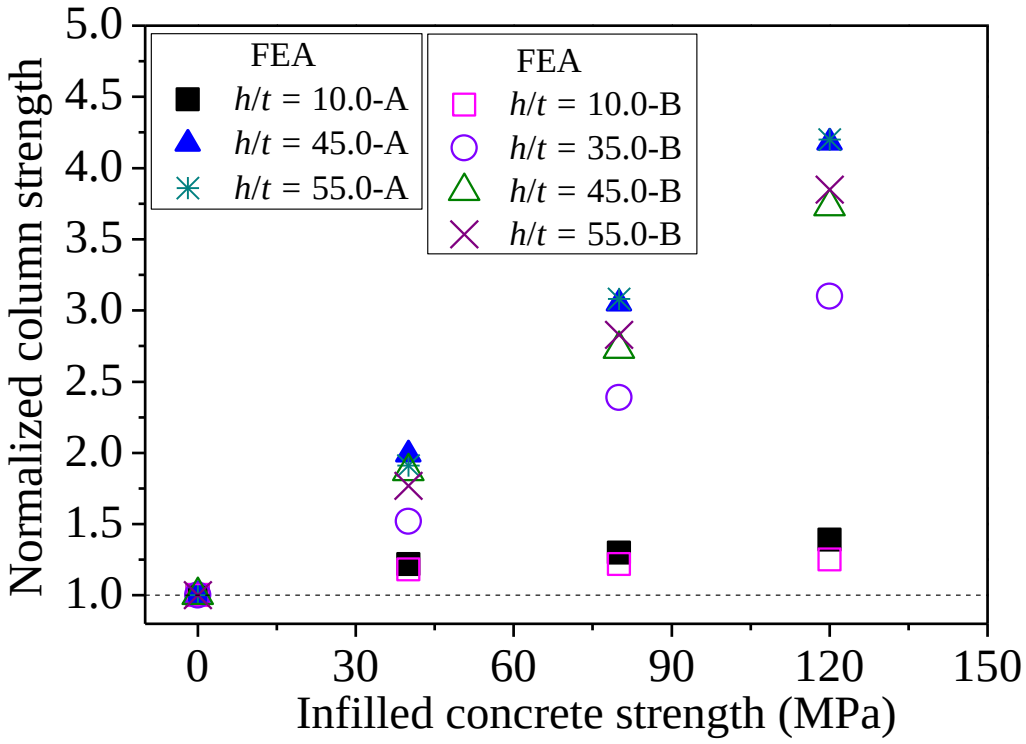

(b) Square sections from FEA results

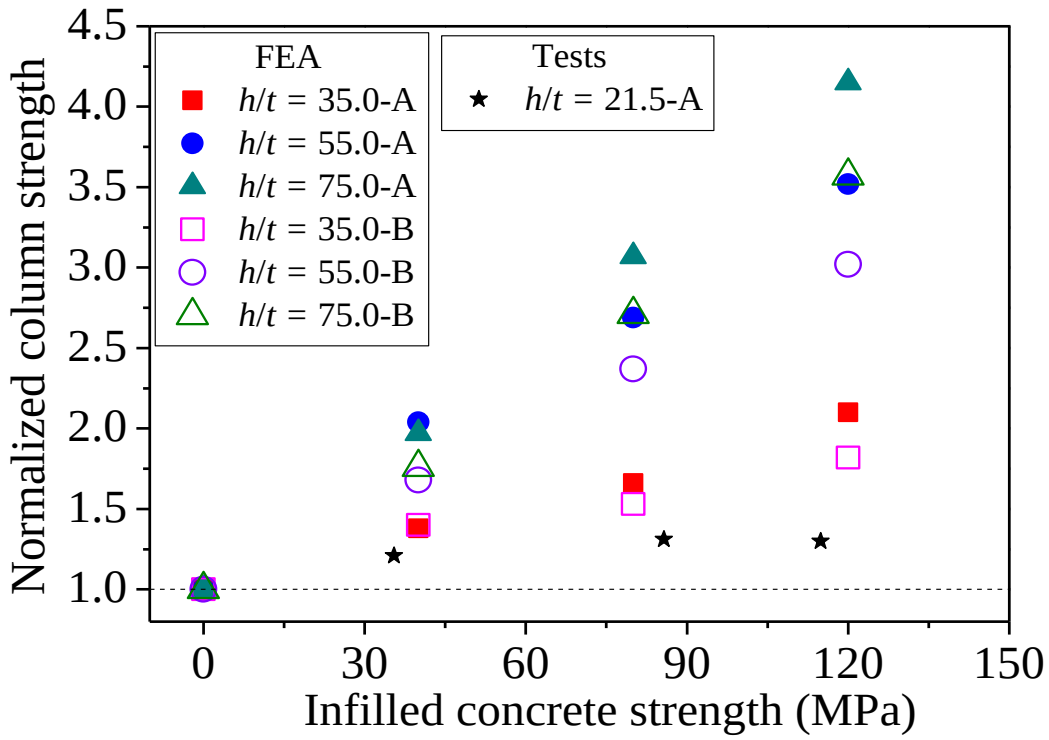

(c) Rectangular sections

Figure 10: Comparison of column strength enhancement with different infilled concrete strengths

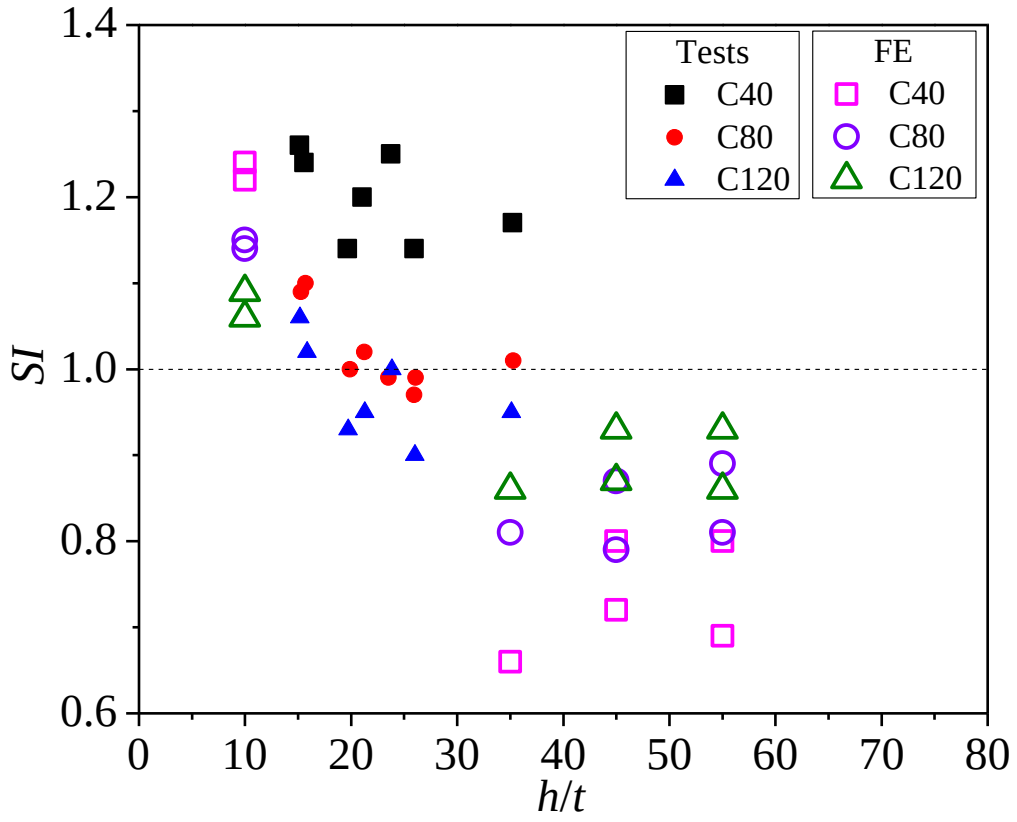

Figure 11: Effects of *h*/*t* on *SI* on concrete-filled CFHSS stub columns with square sections

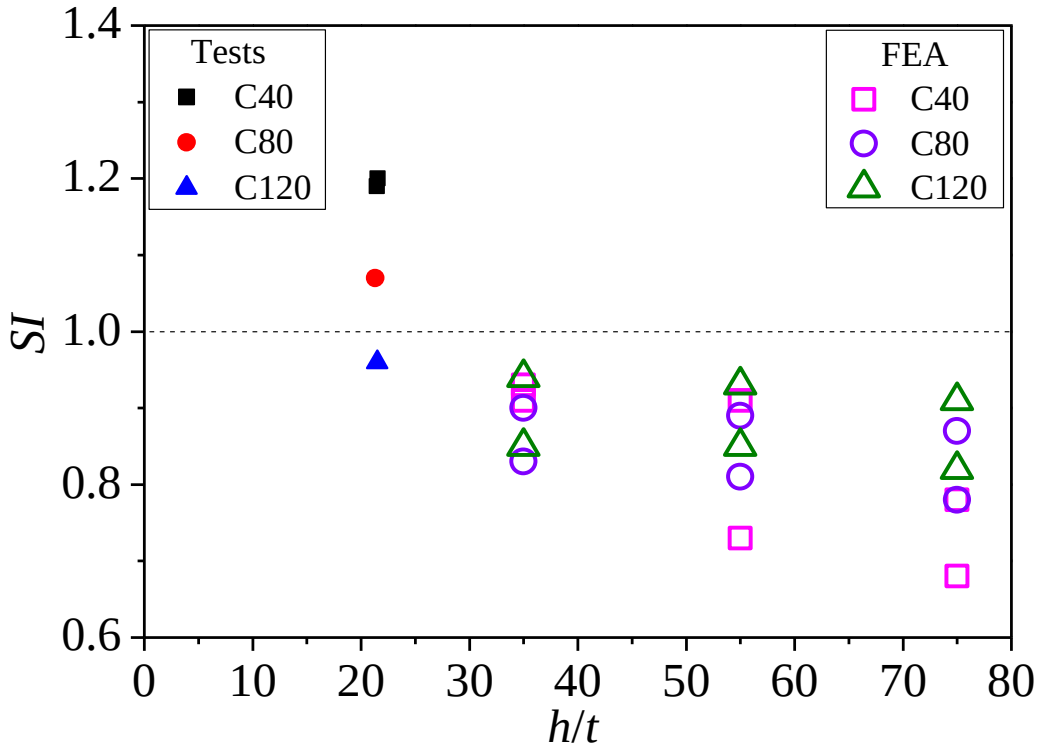

Figure 12: Effects of *h*/*t* on *SI* for concrete-filled CFHSS stub columns with rectangular sections

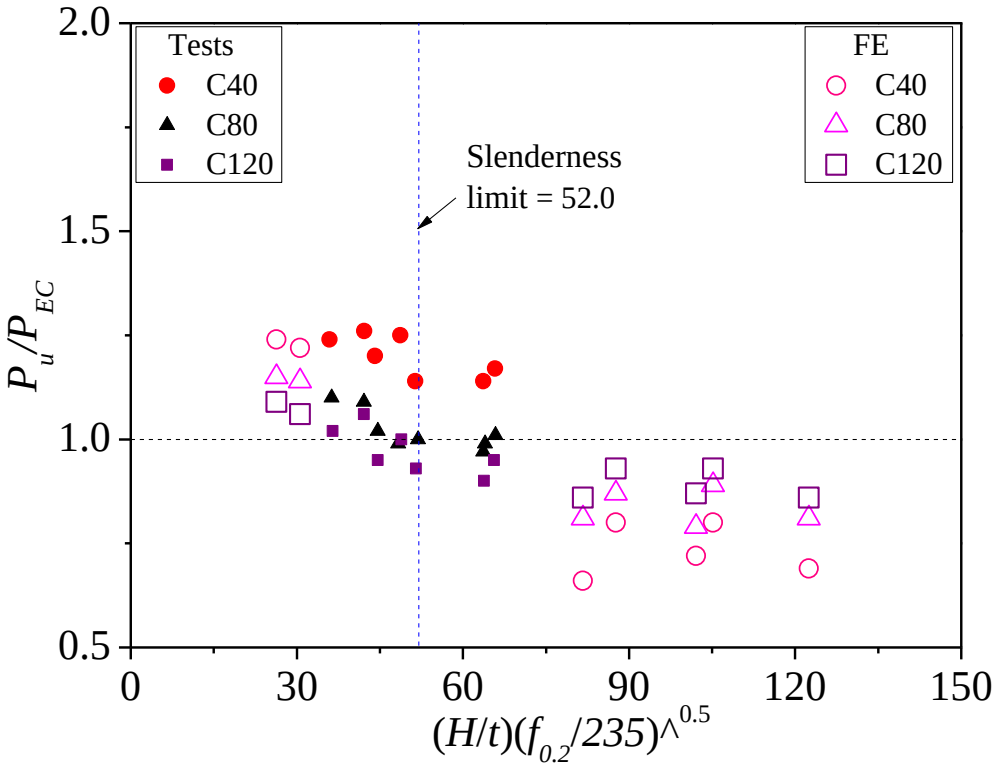

(a) Predictions of P_{EC}

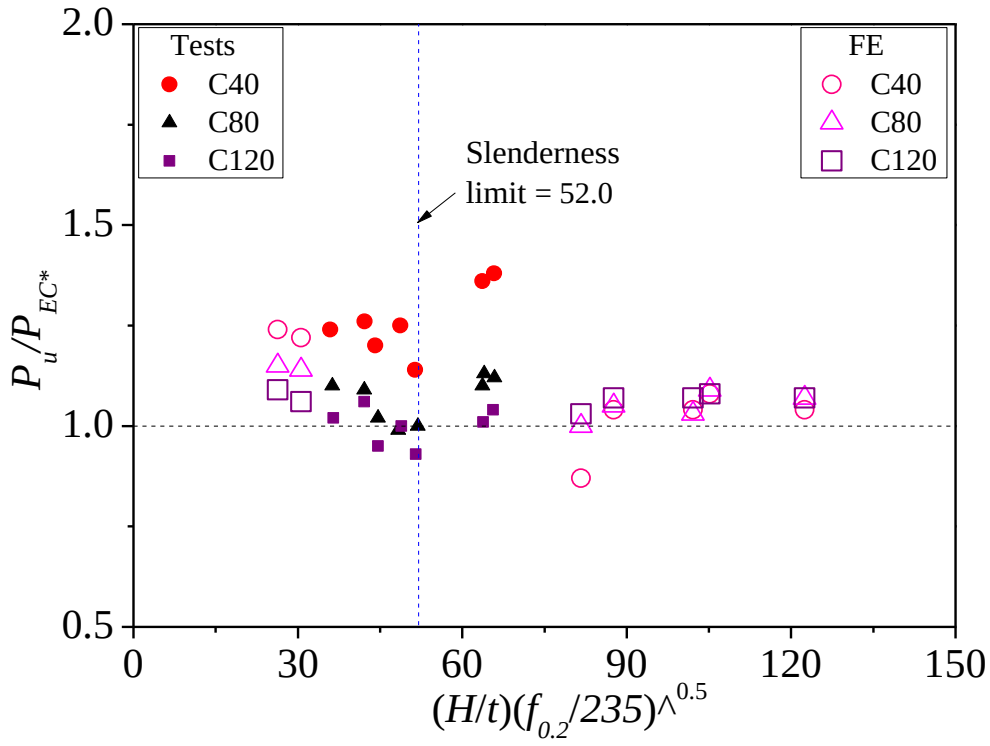

(b) Predictions of P_{EC*} with consideration of effective area

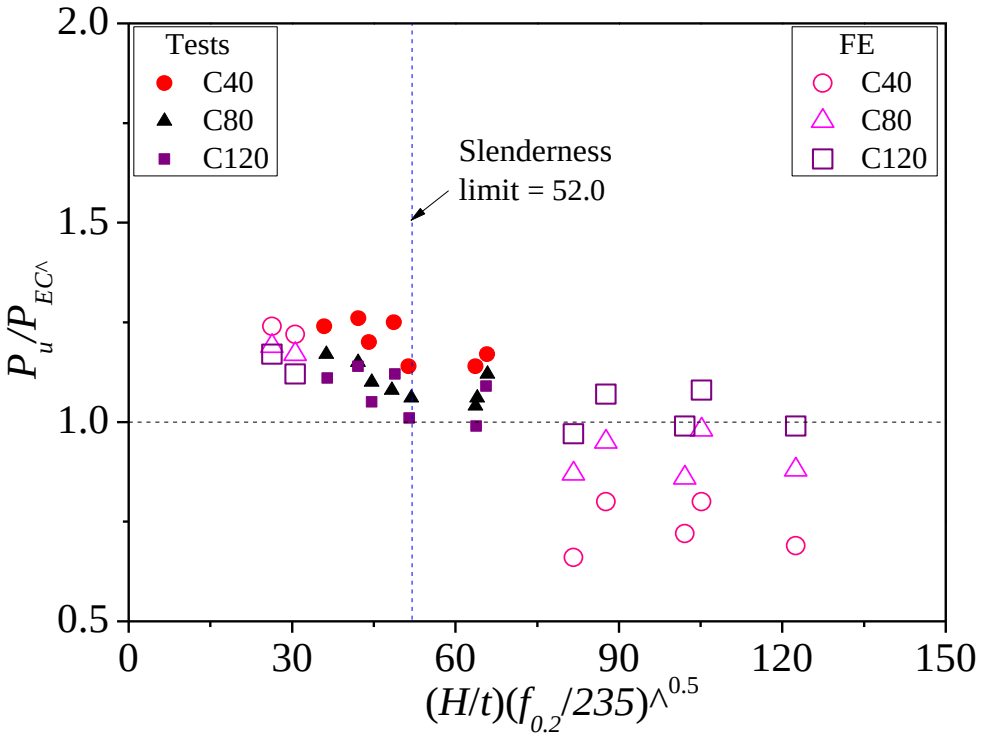

(c) Predictions of $P_{EC\wedge}$ with consideration of effective concrete strength

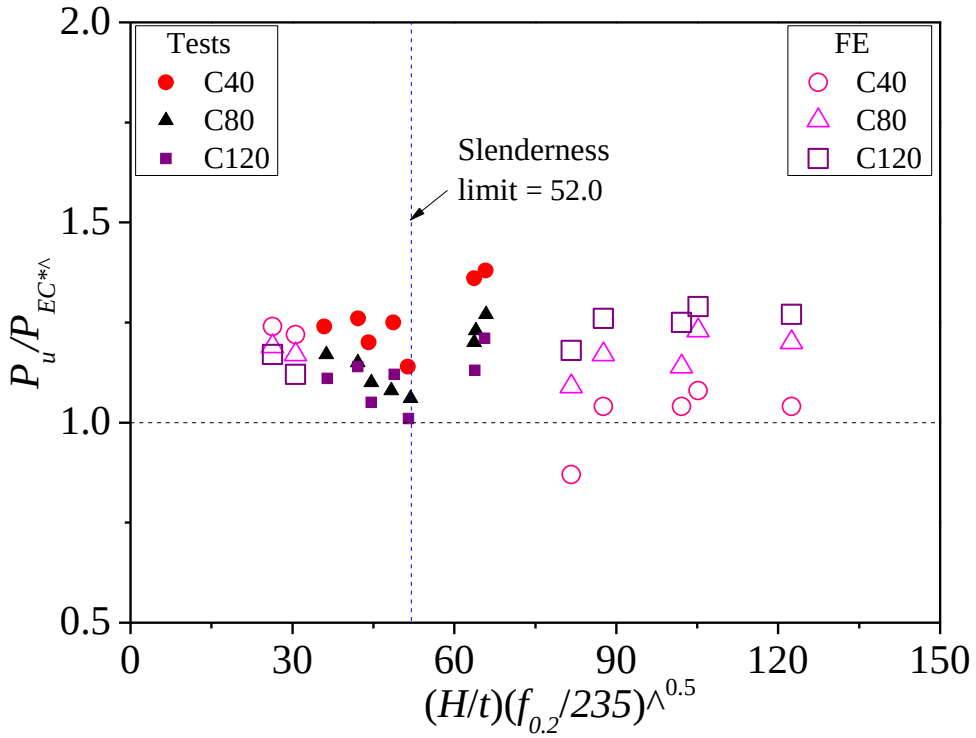

(d) Predictions of $P_{EC*\wedge}$ with consideration of both effective area and effective concrete strength

Figure 13: Assessment of predictions from EC4 [22] for square sections

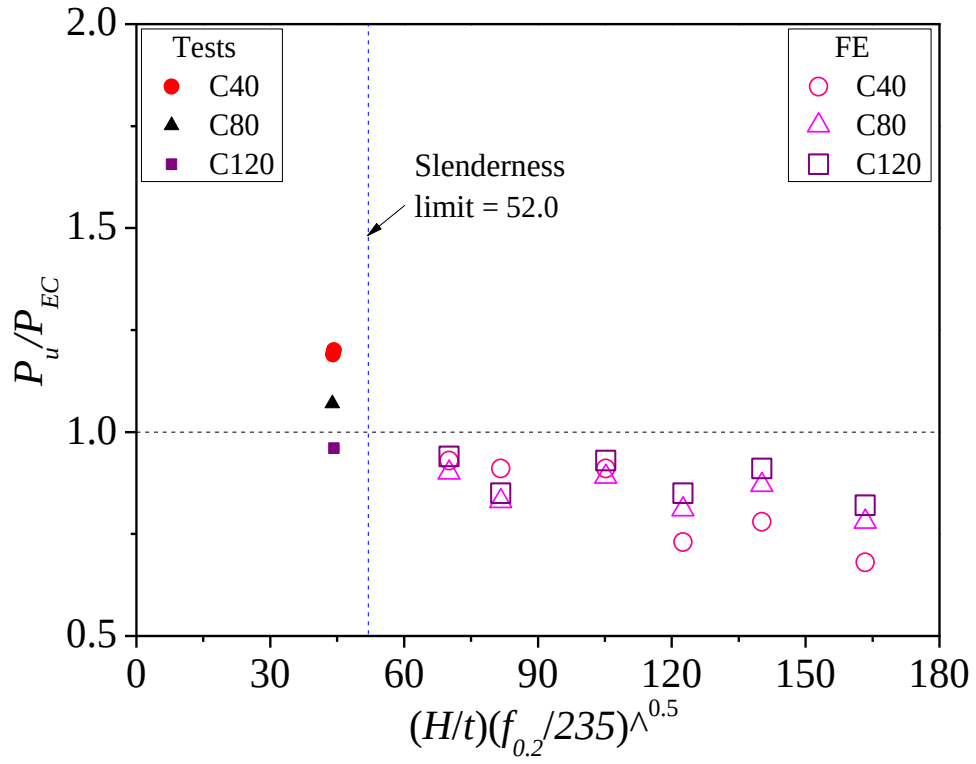

(a) Predictions of P_{EC}

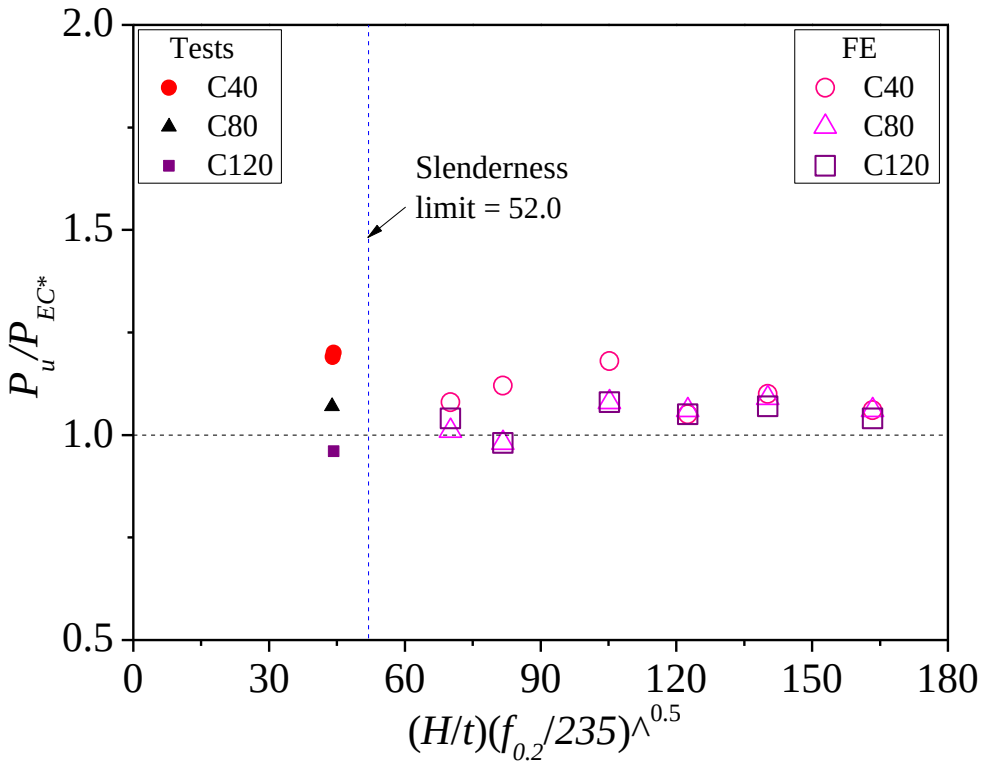

(b) Predictions of P_{EC*} with consideration of effective areas

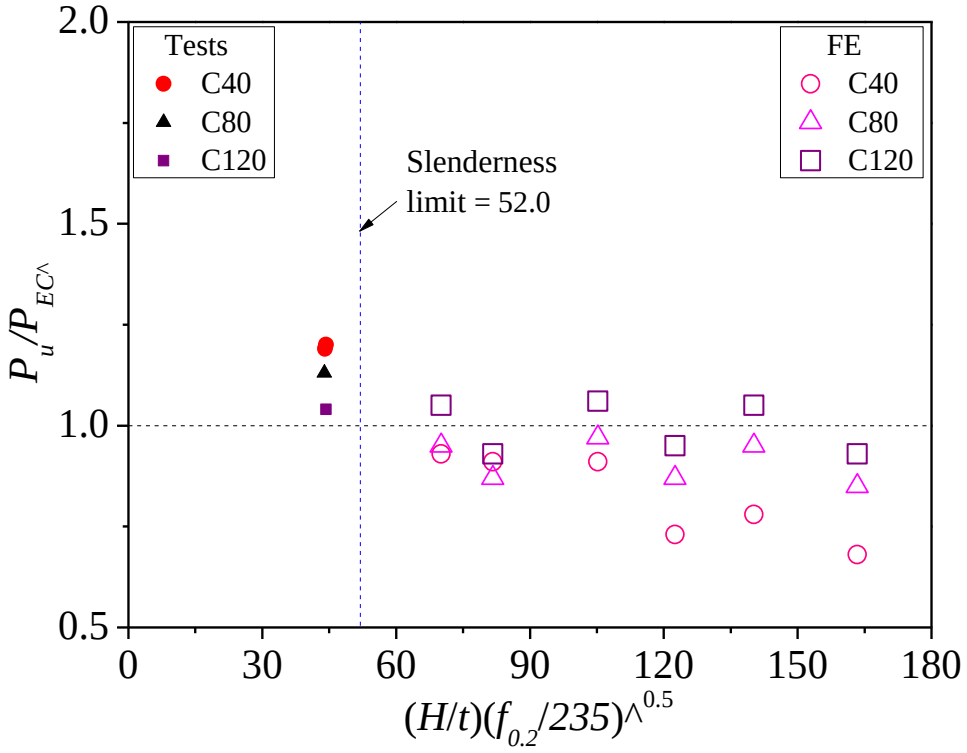

(c) Predictions of $P_{EC^\wedge}$ with consideration of effective concrete strength

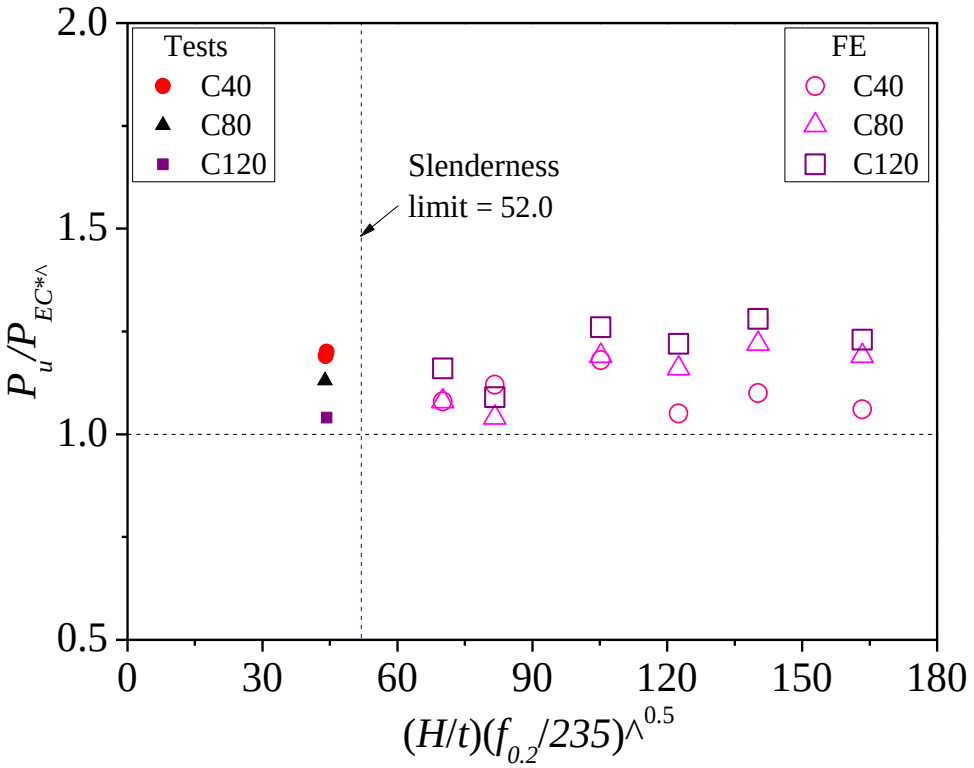

(d) Predictions of $P_{EC^{*\wedge}}$ with consideration of both effective area and effective concrete strength

Figure 14: Assessment of predictions from EC4 [22] for rectangular sections

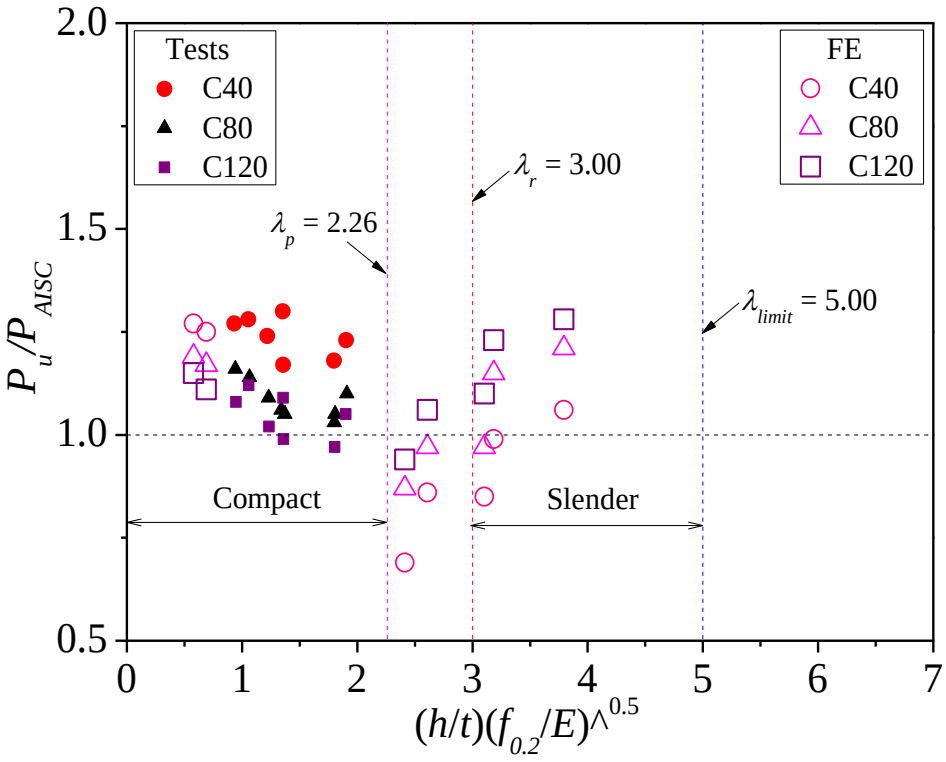

(a) Predictions of P_{AISC}

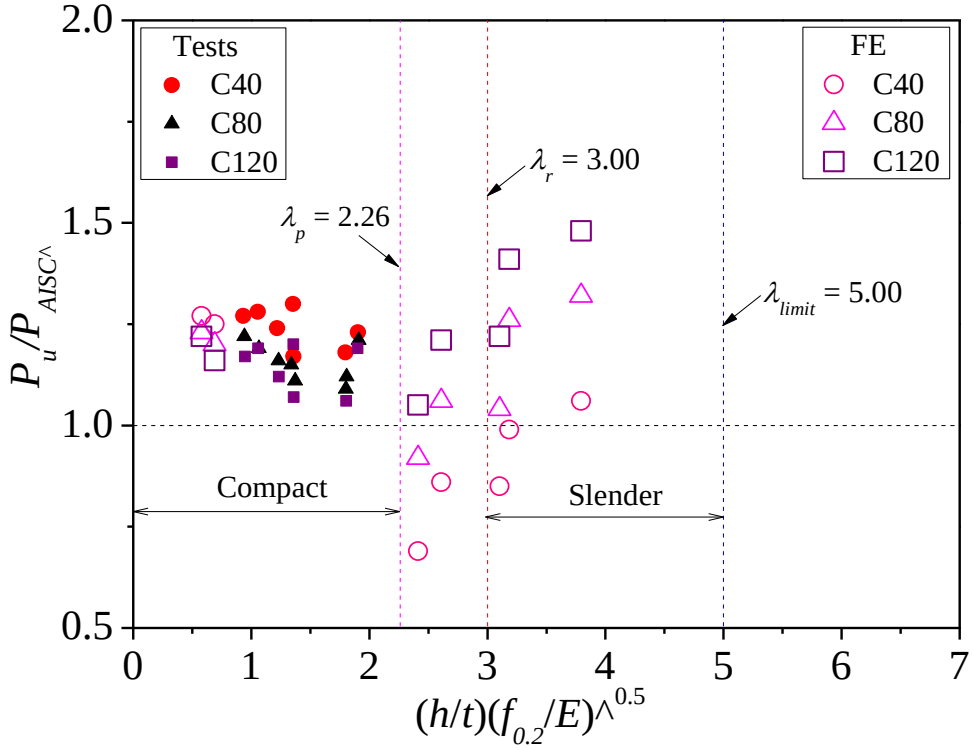

(b) Predictions of $P_{AISC^{\wedge}}$ with consideration of effective concrete strength

Figure 15: Assessment of predictions from AISC [23] for square sections

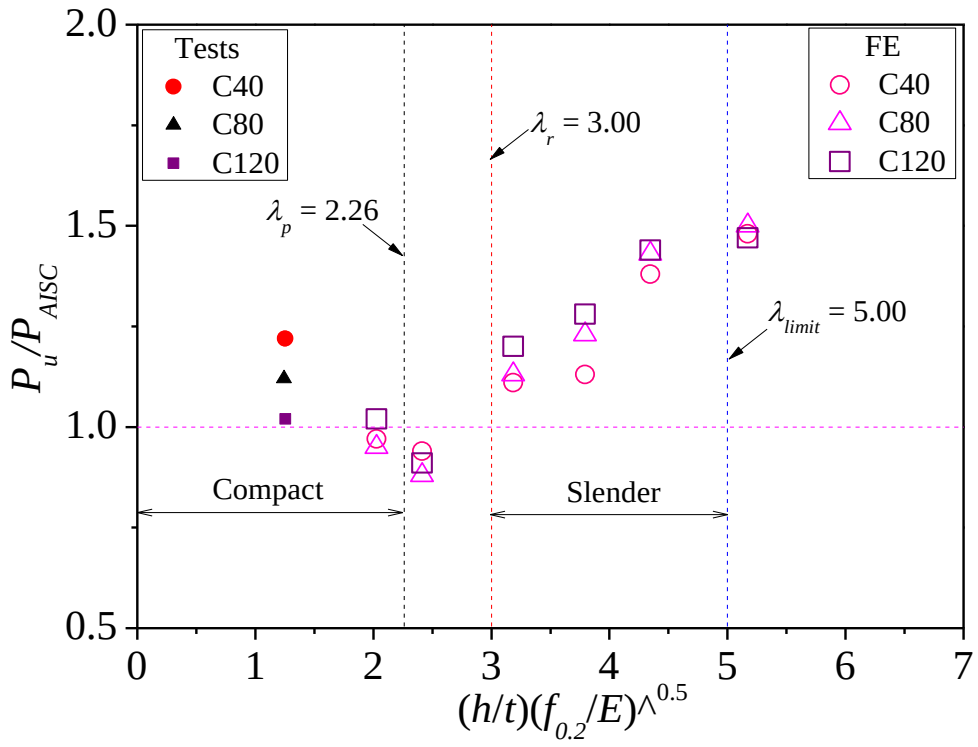

(a) Predictions of P_{AISC}

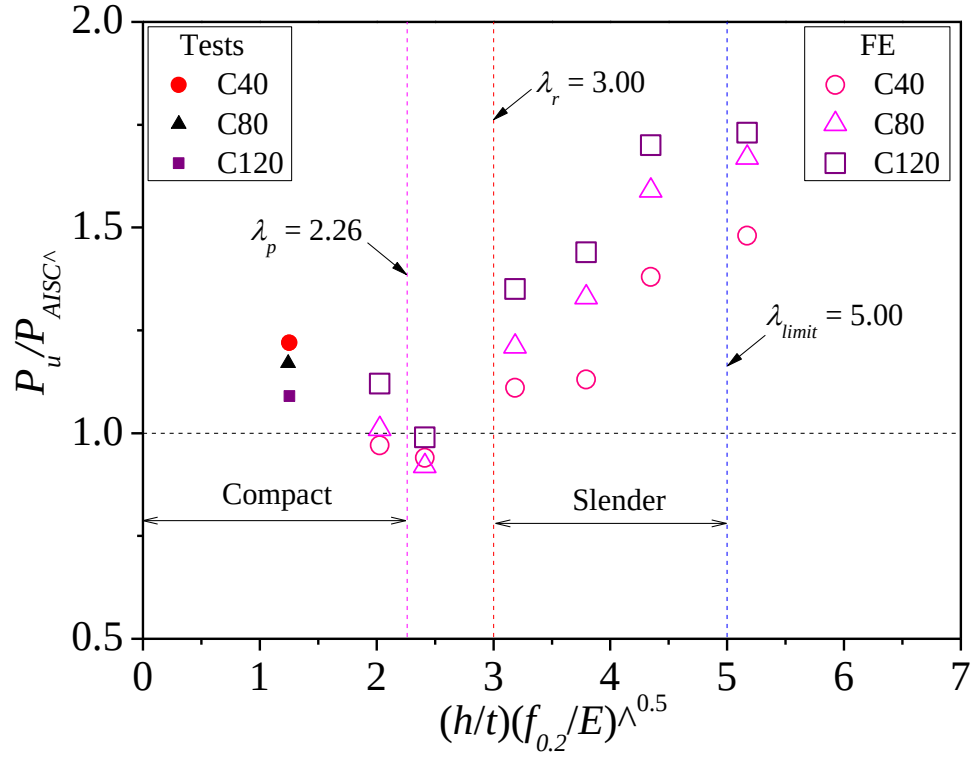

(b) Predictions of $P_{AISC\wedge}$ with consideration of effective concrete strength

Figure 16: Assessment of predictions from AISC [23] for rectangular sections